Journal of Marine Research, 50, 385–420, 1992

Circulation and water mass balance in the Brazil Basin

by Huai-Min Zhang[1] and Nelson G. Hogg[2]

ABSTRACT

Analysis of data from the Levitus (1982) atlas shows that the application of the Montgomery streamfunction to the potential density surfaces induces an error which cannot be ignored in some regions in the ocean. The error arises from the variation of the specific volume anomaly along isopycnal surfaces. By including the major part of this effect, new streamfunctions, named the "pressure anomaly" and "mean pressure" streamfunctions, are suggested for use in potential density coordinates.

By including the variations of specific volume anomaly and pressure along isopycnal surfaces, the inverse model proposed by Hogg (1987) is modified for increased accuracy and then applied to the Brazil Basin to study the circulation, diffusion and water mass balances. The system of equations with constraints of positive diffusivities and oxygen consumption rates is solved by the inverse method. By using multiple tracers and controlling the scale of variation of the diffusion coefficients we are able to construct an overdetermined system whose solution is by a least-square approach. The results indicate that the circulation in the upper ocean is consistent with previous work, but that in the deep ocean differs from some previous analyses. In the NADW depth, we find a coincidence of flow with tongues of water properties. The diffusivities and diapycnal velocities seem stronger in the region near the equator than in the south, with reasonable values. Diffusion plays an important role in the water property balances. Examples show that similar property patterns may result from different processes.

1. Introduction

The investigation of the ocean circulation is important in the study of the heat transport in the ocean and thus the global climate system. Unfortunately, direct measurement of the general circulation, especially in the deep ocean, is extremely difficult. On the other hand, hydrographic data are much more accessible. Thus one primary task for oceanographers is to deduce the ocean circulation from the available hydrographic data. Understanding the physical mechanisms for balances in the water properties is not only itself an important topic, it is also essential for the inference of the circulation from the hydrographic data.

Traditionally, there are two approaches to deducing the ocean circulation from hydrographic data. One is the descriptive method (e.g., Wüst's, 1935 core layer

1. MIT/WHOI Joint Program, Woods Hole, Massachusetts, 02543, U.S.A.
2. Department of Physical Oceanography, Woods Hole Oceanographic Institution, Woods Hole, Massachusetts, 02543, U.S.A.

method), which can only give us flow patterns in a general sense, but not in detail. The other is the dynamic method in which only the relative flows between two surfaces can be calculated. By using the conservation equations for mass, heat, salt, carbon-14 and oxygen in a box model, Wright (1969) determined the deep water transports in the Western Atlantic. More recently, Wunsch (1977) introduced inverse theory to the field of oceanography to determine the reference level velocities. Independently, Stommel and Schott (1977) proposed the β-spiral method to solve essentially the same problem, and this was further extended by Olbers *et al.* (1985). Instead of solving for the reference velocities, Hogg (1987) combined the dynamic method with the conservation laws for the water properties to determine the absolute velocities at all levels simultaneously by the least square fit, or inverse method. In the present work, Hogg's model is first modified to make it more exact for the potential density coordinates, then the model is applied to the Brazil Basin to study the circulation and diffusion processes in that region.

The Brazil Basin contains a rich water mass structure, namely: the central water in the surface; the Antarctic Intermediate Water (AAIW), Circumpolar Water (CPW), Antarctic Bottom Water (AABW) from the south; and the North Atlantic Deep Water (NADW) from the north. All these waters meet in the Brazil Basin, flowing over and mixing with each other to adjust their characteristics. Nevertheless, the exact pathways of the flows and the mechanisms by which the water masses are modified are still unclear. Because of the complicated vertical distributions of the water properties, double diffusion may be effective.

The purpose of this work is to try and answer some of the questions raised above. In Section 2, new streamfunctions for the potential density surfaces (hereafter defined as isopycnal surfaces) are deduced based on the data analysis. Section 3 gives a description of the model and a brief discussion of the basic inverse techniques used in this work. The model results and their analysis are presented in Section 4, followed by a brief summary.

2. Streamfunctions for potential density surfaces

In the ocean it is possible to find surfaces along which the velocities and mixing have their major components while those across are minimized. The conventional choice of such surfaces is the isopycnals (e.g., Montgomery, 1938), while McDougall (1987) has argued more recently for neutral surfaces. In practice, the computation and interpretation of the neutral surfaces are far more difficult than that of the historically used isopycnals. As neutral and isopycnal surfaces coincide at the reference pressure, if the potential densities at different depths are with reference to the different pressures (as in the use of σ_1, σ_2, σ_3, σ_4), the deviation between these two kinds of surfaces should be small. In this work isopycnal surfaces will be used.

Streamfunctions for several different vertical coordinates have been found (for summary, see McDougall, 1989). Nevertheless, exact streamfunctions for isopycnal surfaces do not exist. In most previous works (e.g., Hogg, 1987), the Montgomery streamfunction is applied to isopycnal surfaces by ignoring the variations of specific

volume anomaly along isopycnals. In this section, we will show that this variation may not be negligible in some regions in the ocean, and more accurate streamfunctions for the potential density coordinate will be derived.

In the locally orthogonal potential density coordinates (hereafter, σ represents the *potential* density surfaces, which can be σ_θ or σ_1 to σ_4), the 3-D gradient and divergence operators can be obtained as

$$\nabla A = \hat{i}\frac{\partial A}{\partial x} + \hat{j}\frac{\partial A}{\partial y} + \hat{k}\sigma_z\frac{\partial A}{\partial \sigma} \equiv \nabla_\sigma A + \hat{k}\sigma_z\frac{\partial A}{\partial \sigma} \tag{2.1}$$

$$\nabla \cdot \mathbf{A} = \sigma_z\left[\frac{\partial}{\partial x}\left(\frac{A_1}{\sigma_z}\right) + \frac{\partial}{\partial y}\left(\frac{A_2}{\sigma_z}\right) + \frac{\partial A_3}{\partial \sigma}\right] \equiv \nabla_h \cdot \mathbf{A} + \sigma_z\frac{\partial A_3}{\partial \sigma} \tag{2.2}$$

where ∇_σ and ∇_h are the 2-D lateral gradient and divergence operators. The lateral gradients are taken along the isopycnals. The relation between the 2-D gradient operators in the z-coordinate and the σ-coordinate is

$$\nabla_z A = \nabla_\sigma A - \frac{\partial A}{\partial z}\nabla_\sigma z. \tag{2.3}$$

Using Eq. (2.3) and the hydrostatic equation, the geostrophic relation in the z-coordinate, $\hat{k} \times f\mathbf{u} = -1/\rho\nabla_z p$, can be transformed to an arbitrary vertical s-coordinate (e.g., $s = \sigma$) as

$$\hat{k} \times f\mathbf{u} = -[\alpha\nabla_s p - \nabla_s \int^p \alpha\, dp] \tag{2.4}$$

$$= -[\delta\nabla_s p - \nabla_s \int^p \delta\, dp] \tag{2.5}$$

where α and δ are specific volume and its anomaly.

For certain choices of s, the known streamfunctions can be derived from (2.4) or (2.5) directly. For example, for $s = z$, p is the streamfunction for $\rho f\mathbf{u}$; for $s = p$, the dynamic height $-\int^p \delta\, dp \equiv \psi_p$ or the geopotential $-\int^p 1/\rho\, dp$ is the streamfunction for $f\mathbf{u}$; for $s = \delta$, the $\psi_M = p\delta - \int^p \delta\, dp$ is the Montgomery streamfunction for $f\mathbf{u}$ and for $s = \alpha = 1/\rho$, the $\psi = p/\rho - \int^p dp/\rho$ is the Montgomery streamfunction for $f\mathbf{u}$. Note that the so called streamfunction here is only a representation of the geostrophic relation for the horizontal geostrophic velocity. It is not a streamfunction in the conventional sense in which 2-D nondivergence is implied unless the Coriolis parameter is a constant.

For the isopycnal surfaces ($s = \sigma$), Eq. (2.5) can be rewritten as

$$\hat{k} \times f\mathbf{u} = -[\nabla_\sigma\left(\delta p - \int^p \delta\, dp\right) - p\nabla_\sigma\delta], \tag{2.6}$$

i.e., as well as the two components of the Montgomery streamfunction, there is an extra or error term $ER_M = p\nabla_\sigma\delta$, proportional to p. Analysis of these terms between

two isopycnals $\sigma_1 = 31.8$ and 32.3 in the Mediterranean Water tongue region (the area analyzed by Hogg, 1987) using the Levitus atlas values (Levitus, 1982) indicated that, although each component of the two gradient terms of the Montgomery streamfunction can have a magnitude an order larger than that of the error term, as the two components usually have opposite signs, their combination is greatly reduced and generally of the same magnitude as the error term. Therefore we believe that the term $p\nabla_\sigma\delta$ may not be negligible in calculating the geostrophic velocity.

Defining the pressure anomaly as $p' = p - \bar{p}$, where $\bar{p}$ is the lateral mean on the s-surface, then Eq. (2.5) is identical to

$$\hat{k} \times f\mathbf{u} = -\left[\delta\nabla_s p' - \nabla_s \int^p \delta\, dp\right] \tag{2.7}$$

$$= -\left[\nabla_s\left(p'\delta - \int^p \delta\, dp\right) + p'\nabla_s\delta.\right. \tag{2.8}$$

If we now define a streamfunction as

$$\psi_a = p'\delta - \int^p \delta\, dp, \tag{2.9}$$

labeled with pressure *anomaly* streamfunction, then the error on the use of ψ_a on the s-surface will be $ER_a = p'\,\nabla_s\,\delta$, proportional to p'. Generally, $ER_a/ER_M = p'/p \ll 1$. Furthermore, the Levitus atlas values shows that

$$\left|\frac{p'\nabla_\sigma\delta}{\nabla_\sigma(p'\delta - \int^p \delta\, dp)}\right| \sim O(10^{-2} \sim 10^{-1}).$$

Consequently we conclude that the ψ_a is a reasonably good streamfunction for the isopycnal surfaces, with the errors in velocity of at most 10% or less.

Another expression for the streamfunction for the gently sloping s (e.g. $s = \sigma$) surfaces can be obtained by using the approximation

$$\begin{aligned}\int_{p_1}^{p_2} \delta\, dp &= \int_{\bar{p}_1}^{\bar{p}_2} \delta\, dp - \int_{\bar{p}_1}^{\bar{p}_1+p_1'} \delta\, dp + \int_{\bar{p}_2}^{\bar{p}_2+p_2'} \delta\, dp \\ &\approx \int_{\bar{p}_1}^{\bar{p}_2} \delta\, dp - \delta_1 p_1' + \delta_2 p_2'.\end{aligned} \tag{2.10}$$

Then Eq. (2.5) can be developed to

$$\begin{aligned}\hat{k} \times f(\mathbf{u}_1 - \mathbf{u}_2) &= -\left[\nabla_s \int_{p_1}^{p_2} \delta\, dp + \delta_1\nabla_s p_1 - \delta_2\nabla_s p_2\right] \\ &= -\left[\nabla_s \int_{\bar{p}_1}^{\bar{p}_2} \delta\, dp - p_1'\nabla_s\delta_1 + p_2'\nabla_s\delta_2\right].\end{aligned} \tag{2.11}$$

The last two terms on the RHS are exactly the error terms neglected in the definition

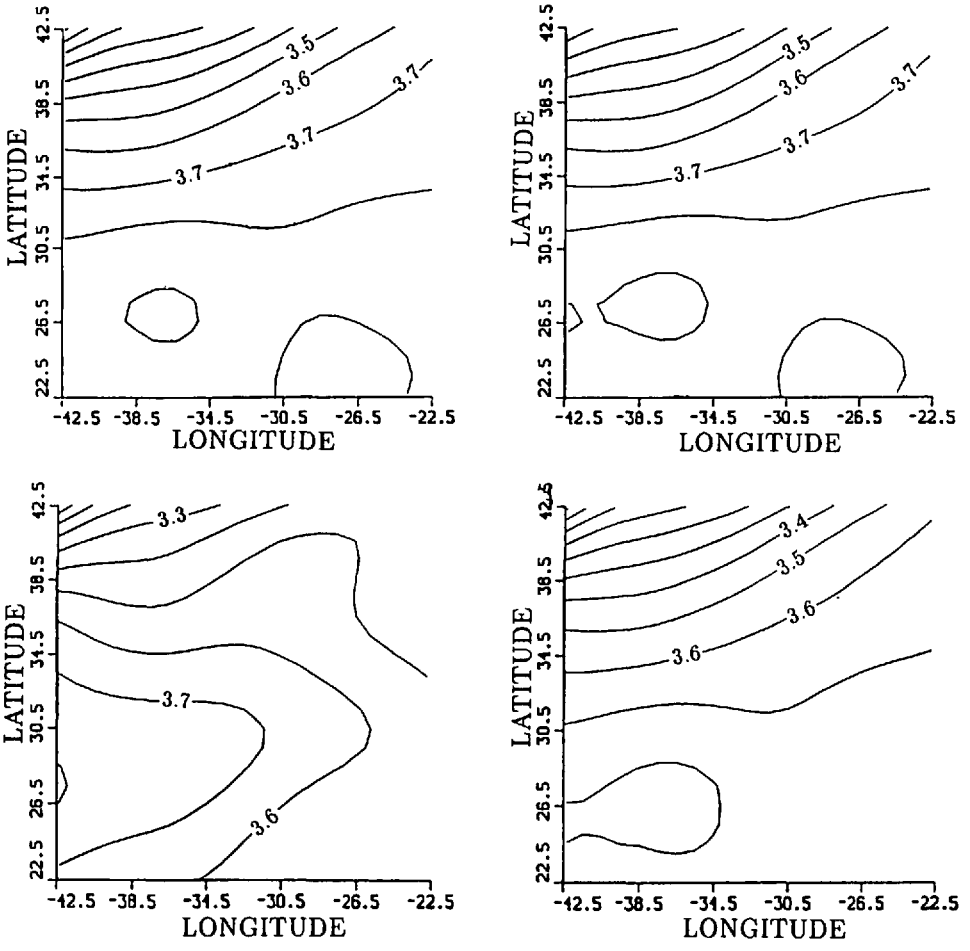

Figure 1. Various streamfunctions for different vertical coordinates. (a) ψ_a between $\sigma_1 = 31.8$ and $\sigma_1 = 32.3$; (b) $\bar{\psi}$ between $\sigma_1 = 31.8$ and $\sigma_1 = 32.3$; (c) ψ_M between $\sigma_1 = 31.8$ and $\sigma_1 = 32.3$; (d) ψ_M between $\delta = 89.0$ and $\sigma_1 = 52.0$; (e) $\bar{\psi}$ between $\delta = 89.0$ and $\sigma_1 = 52.0$; (f) ψ_p between $p = 759.6$ and $p = 1335.9$.

of ψ_a, and for the same reason can be ignored here. Hence the expression for the streamfunction $\bar{\psi}$ (labeled as the *mean* pressure streamfunction) is obtained as

$$\bar{\psi} = \int_{\bar{p}_1}^{\bar{p}_2} \delta \, dp. \tag{2.12}$$

To show the effectiveness of the use of the pressure *anomaly* and *mean* pressure streamfunctions, the ψ_a's and $\bar{\psi}$'s for the isopycnals and the $\bar{\psi}$'s for the specific volume anomaly surfaces in the Mediterranean Water tongue region are computed from the Levitus atlas values and displayed in Figure 1. Also shown in this figure are the *exact* streamfunctions for the specific volume anomaly surfaces (Montgomery streamfunction) and for the pressure surfaces (Dynamic Height) as well as the

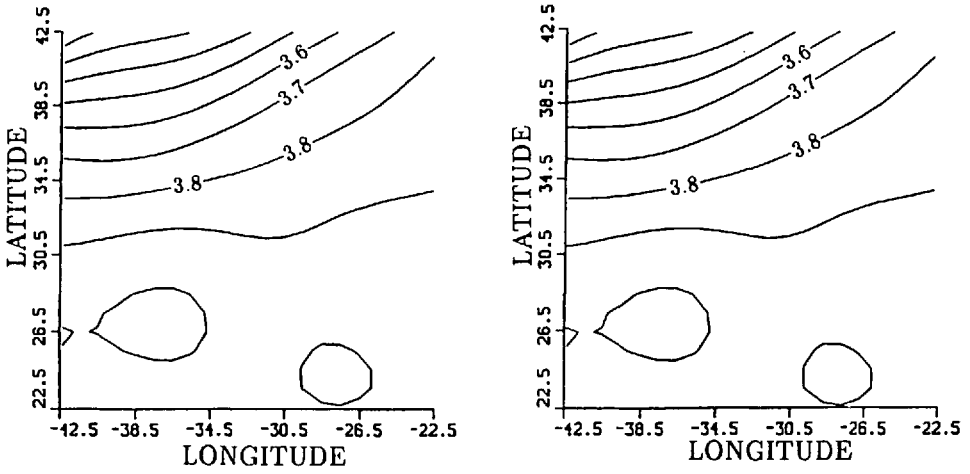

Figure 1. (Continued)

Montgomery streamfunction applied to the isopycnal surfaces. (The two values for δ and p in Fig. 1 correspond to their means on the two isopycnals.) It can be seen that all the streamfunctions except the Montgomery streamfunction applied on the isopycnals show similar flow patterns. We can see that the errors in the use of the Montgomery streamfunction on the isopycnals are large in the southern part of the region. It also shows the uses of ψ_a and $\bar{\psi}$ on the isopycnal surfaces are extremely good. In this work we will use the ψ_a as the streamfunction.

3. Description of the model

The model used here is basically the one proposed by Hogg (1987) modified to include the sloping effect of specific volume anomaly and pressure along isopycnals. The assumptions and controlling equations are:

a. Hydrostatic and geostrophic balances—dynamic equation.

$$\psi_k(x,y) - \psi_{k+1}(x,y) = \int_{p_k}^{p_{k+1}} \delta \, dp + p'_k\delta_k - p'_{k+1}\delta_{k+1}, \qquad k = 1, 2, \ldots, N-1 \quad (3.1)$$

where N is the level number of the isopycnals in the model.

b. Mass conservations at the grid points—continuity equation. In the σ-coordinate, the continuity equation (3-D nondivergence) can be written as (Hogg, 1987)

$$\nabla_h \cdot \mathbf{u}_g - \frac{\beta}{f_0} v_g + \sigma_z \frac{\partial w^*}{\partial \sigma} = 0 \quad (3.2)$$

where f_0 is a local constant and $\mathbf{u}_g$ is laterally nondivergent ($\nabla_\sigma \cdot \mathbf{u}_g \equiv 0$), defined as $f_0\mathbf{u}_g = f\mathbf{u}$, and $\mathbf{u}$ represents the 2-D lateral velocity. w^* is the *diapycnal* velocity.

c. Mass or potential vorticity conservation between isopycnals—integrated vorticity equation. By considering the variations of specific volume anomaly and pressure along isopycnals, the integration of the continuity equation between two isopycnals yields

$$[w^*]_{k+1}^k - 10^{-4}[\nabla_\sigma(\mathbf{u}_g p)]_{k+1}^k - 10^{-4}\frac{\beta}{f^2}\frac{p_{k+1}-p_k}{2}(\psi_{k_x}+\psi_{k+1_x})$$

$$= -10^{-4}\frac{\beta}{f^2}\frac{p_{k+1}+p_k}{2}\frac{\partial}{\partial x}DYN1_k + \frac{10^{-4}\beta}{f^2}\frac{\partial}{\partial x}DYN2_k \qquad (3.3)$$

$$+\frac{10^{-4}}{f}[p(p_x\delta_y - p_y\delta_x)]_k^{k+1} - \frac{10^{-4}\beta}{f^2}[\delta p p_x]_k^{k+1}$$

where

$$DYN1_k \equiv \psi_k - \psi_{k+1} = \int_k^{k+1}\delta\, dp - p'_{k+1}\delta_{k+1} + p'_k\delta_k, \qquad (3.4)$$

$$DYN2_k \equiv \int_k^{k+1} p\delta\, dp. \qquad (3.5)$$

and all the variables are in SI units.

d. The conservation equations for water properties. The equation for concentration C in the σ-*coordinate* is derived as (Hogg, 1987)

$$\nabla_h\cdot(\mathbf{u}_g C) - \frac{\beta v_g C}{f_0} + \sigma_z\frac{\partial}{\partial\sigma}(w^*C) = \nabla_h\cdot A\nabla_\sigma C + \sigma_z\frac{\partial}{\partial\sigma}\left(K\sigma_z\frac{\partial C}{\partial\sigma}\right) - \lambda C \qquad (3.6)$$

where A and K are the isopycnal and diapycnal diffusivities respectively; λ is the consumption rate for oxygen only. The properties used here are potential temperature, salinity and oxygen. To reduce solution errors, the continuity equation is used to transform this into an equation for the concentration anomaly $C' = C - \overline{C}$, where $\overline{C}$ is the mean of C on the isopycnals.

Along isopycnals, the eddy diffusivities are generally much greater than the molecular ones, thus we may assume that they are the same for all the water properties. The diapycnal diffusivities for heat and salt may be different since double diffusion may also be important in the diapycnal mixing.

e. Data. The hydrographic data used are the climatalogical hydrographic atlas prepared by Levitus (1982). Our modeled area sits in the Brazil Basin, extending from 3S to 27S and from 32W to 18W (Fig. 2). In order to study the flow patterns and balances of the major water masses, eight isopycnal surfaces are chosen in the vertical (Table 1 and Fig. 3). The Levitus atlas reports the values of the water properties at the standard levels, thus a piecewise polynomial (the B-spline, see de

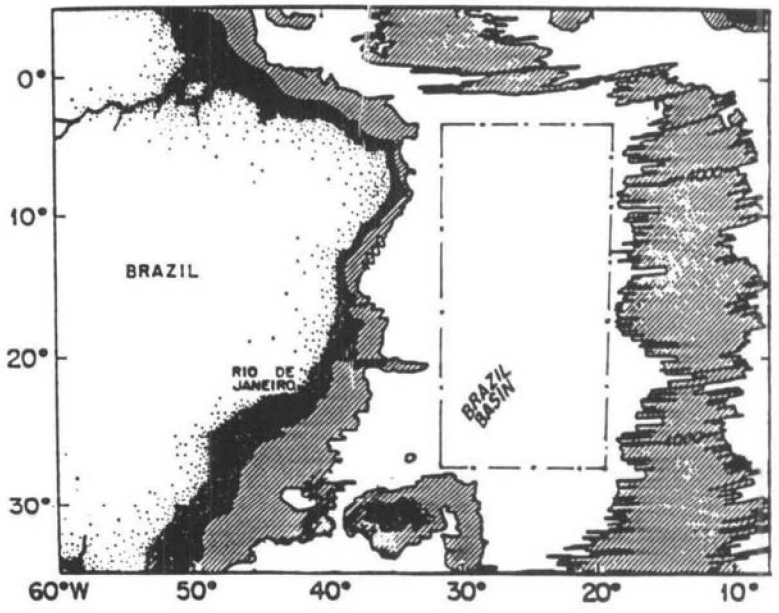

Figure 2. Modeled area (dot-dashed lines) in this work.

Boor, 1978) interpolation is used to generate the values of water properties and their vertical derivatives on the isopycnals (Fig. 4).

Pressure varies most on the upper isopycnals, as shown in Figure 4a and Figure 4b. These large variations dominate the flow patterns, although pressure is not exactly the streamfunction for isopycnals (see Section 4a for more detail). The isotherms for Near Surface Water and AAIW have closed warm and cool centers (Fig. 4c, 4d), those for the CPWs have apparent zonal distributions (Fig. 4e, 4f), while those for the NADWs have tongue-like structures (Fig. 4g). These property fields will be further analyzed in Section 4 in conjunction with the analysis of the results.

Table 1. The eight isopycnals and the water masses.

Level numbers	Isopycnal values	Water masses	Depth ranges (m)
1	$\sigma_0 = 26.88$	Near Surface Water	250-550
2	$\sigma_1 = 31.88$	AAIW	700-900
3	$\sigma_1 = 32.08$	upper CPW	1050-1150
4	$\sigma_1 = 32.28$	lower CPW	1350-1500
5	$\sigma_2 = 36.94$	interface	1800-1900
6	$\sigma_2 = 37.00$	upper NADW	2250-2400
7	$\sigma_3 = 41.46$	mid NADW	2700-2950
8	$\sigma_3 = 41.50$	lower NADW	3350-3500

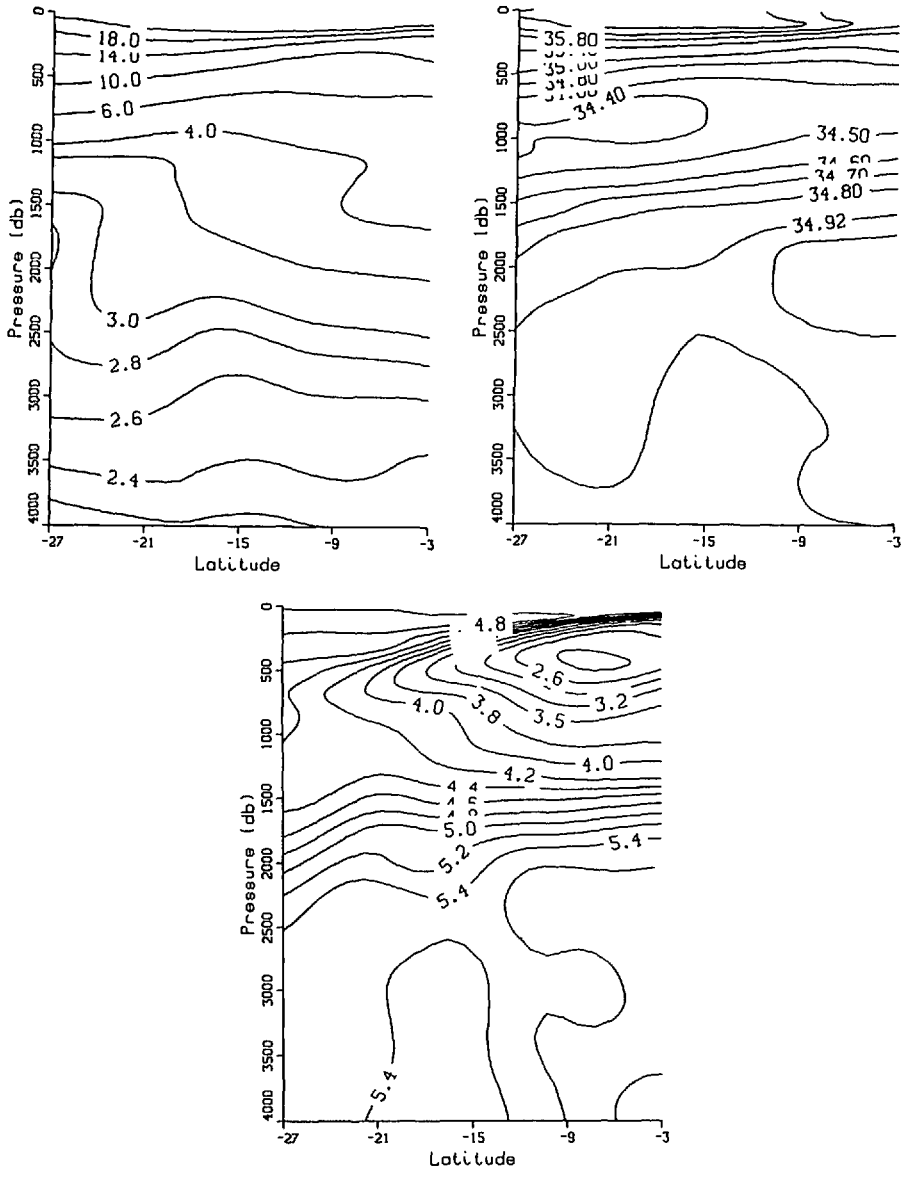

Figure 3. Property contours along section 24.5W. (a) potential temperature; (b) salinity; (c) oxygen.

f. Difference equations and additional constraints. The equations are written in the centered finite difference form on the grid scheme shown in Figure 5. Grid steps are 2° in latitude and longitude, and varying in the vertical. Then equations are in the matrix form

$$G \times X = Y, \tag{3.7}$$

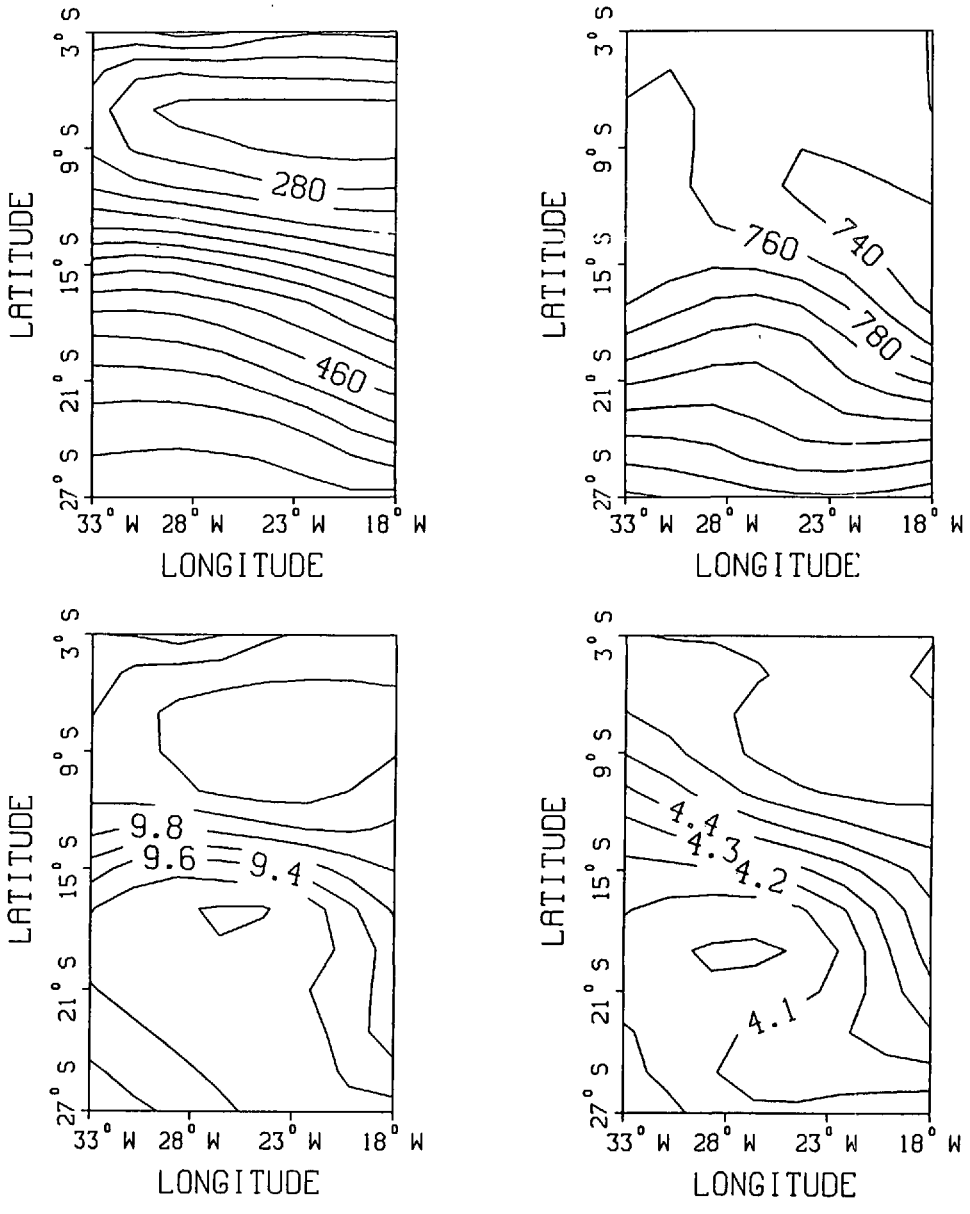

Figure 4. Property contours on the isopycnals. (a) p on level 1 and (b) p on level 2, contour interval (C.I.) = 20 db; (c) θ on level 1, C.I. = 0.2°C; (d) θ on level 2, C.I. = 0.1°C; (e) θ on level 3, C.I. = 0.1°C; (f) θ on level 4, C.I. = 0.1°C; (g) θ on level 6, C.I. = 0.04°C; (h) O_2 on level 1, C.I. = 0.2 ml/l.

where G is the coefficient matrix, X is the vector containing the unknowns, and Y is the RHS including the known inhomogeneous terms. This system is solved by the inverse method, which will be discussed below.

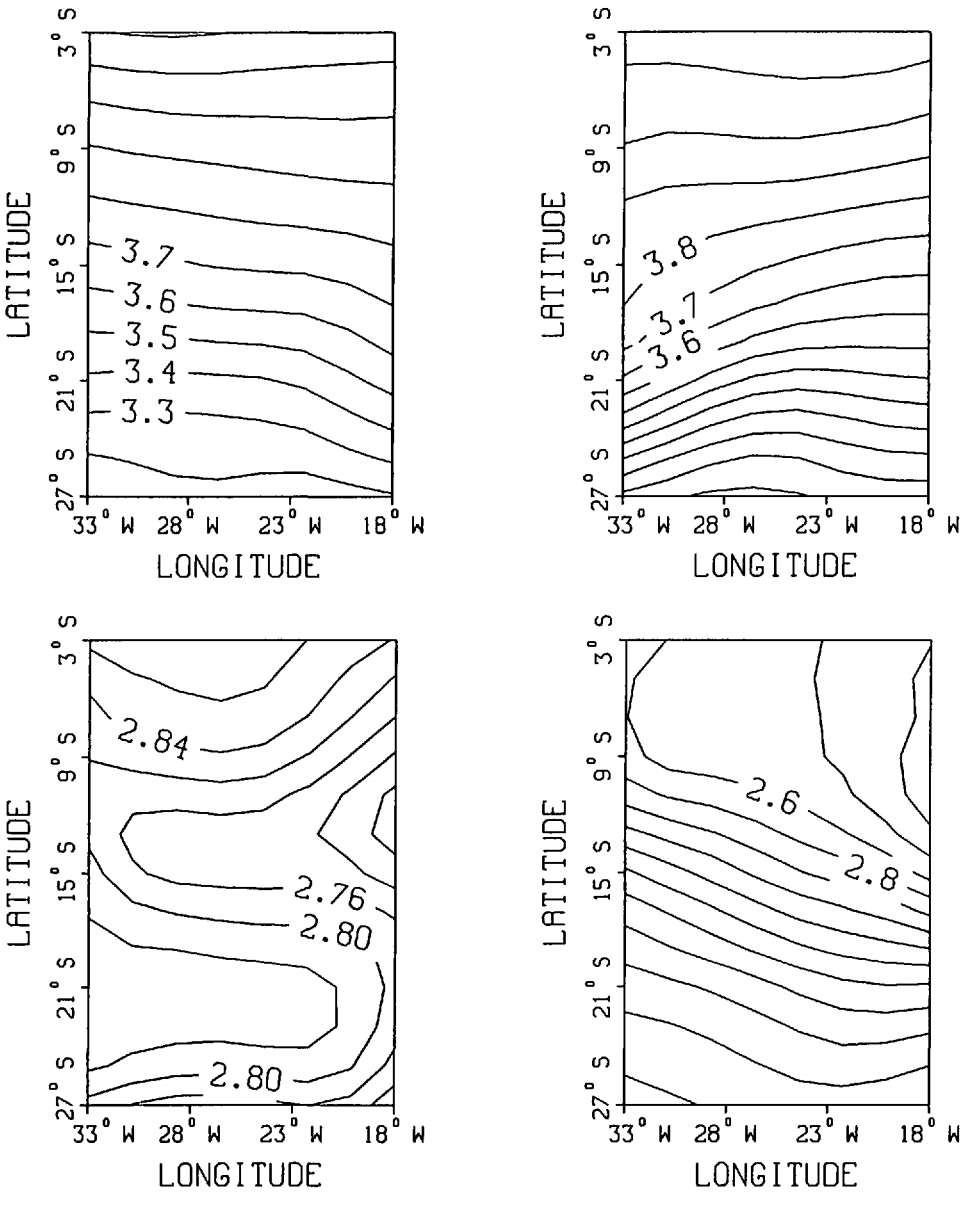

Figure 4. (Continued)

The eddy diffusivities (A, K) vary in space, and this has pseudo-dynamic effects on water property distributions (Armi, 1979; Armi and Haidvogel, 1982). In this work, we parameterize the diffusive parameters as the third order discrete Tchebychev polynomials of x and y whose coefficients may vary from level to level. Based on the assumption that all the eddy diffusive processes are dissipative, it is required that

$$A, K, \lambda > 0. \tag{3.8}$$

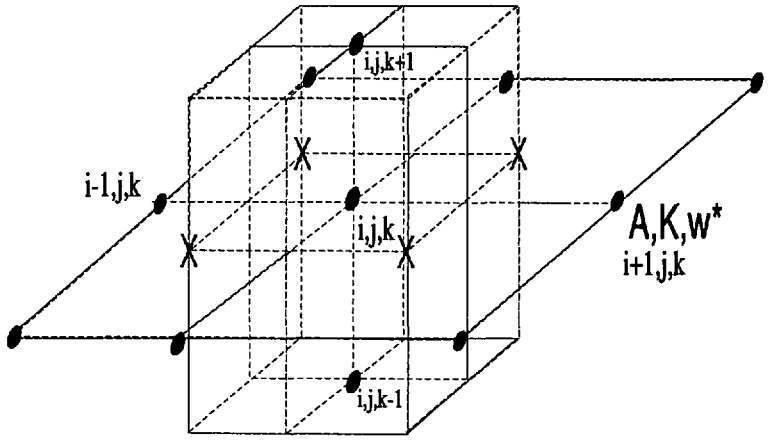

Figure 5. Staggered grid for the centered difference forms of the governing equations. Water properties and diffusive parameters are at · points, and streamfunctions are at X points.

By definition, there is an arbitrary additive constant in the streamfunction, and we can set this constant equal to zero at a fixed location (x_0,y_0). If the lateral grids are *ngx* by *ngy* and the vertical level number is *Nlev* (*ngx* = 8, *ngy* = 13, *Nlev* = 8 here), then the unknown number for streamfunction is *Nlev* × [(*ngx* − 1)(*ngy* − 1) − 1]. If the polynomial degree for the diffusive parameters is *npl* (*npl* = 3 here), then the number of the unknown coefficients for each diffusivity on each isopycnal is (*npl* + 1)(*npl* + 2)/ 2. Thus the unknown number is 644 for the Purely Advective Model, 984 for the Advective-Diffusive Model, and 1064 for the Double-Diffusive Model. The equation number is 2627 for the Purely Advective Model, and 3155 for the models with diffusion so the problem, in principle, is overdetermined.

g. Equation scaling. For the least-squares approach the equations should be scaled by the standard errors of their residuals (see Wunsch, 1978 or Hogg, 1987 for general discussions). In our model, there are eight vertical isopycnal levels with the first one in the thermocline. Write the conservation equation in the form of $\mathbf{u} \cdot \nabla C =$ *other terms.* Note that C is the ensemble mean in theory, and in practice there are two components in it: the climatological mean C_m and the error c' due to the limited sample from which it was obtained and, possibly, measurement errors. Similarly, $\mathbf{u} = \mathbf{U}_m + \mathbf{u}'$. Then the above expression becomes

$$\mathbf{U}_m \cdot \nabla C_m = \textit{other terms} - \mathbf{U}_m \cdot \nabla c' - \nabla C_m \cdot \mathbf{u}' - \mathbf{u}' \cdot \nabla c'. \qquad (3.9)$$

Generally flows and gradients of θ and S in the thermocline are much greater than those in the deep ocean. Thus unless the noise c' and $\mathbf{u}'$ in the thermocline are much smaller than that in deep ocean, the equations should be weighted by factors of $1/(C_{max} - C_{min})_k$. Expecting that all the velocities below the thermocline have the same magnitude, the equations in the thermocline are scaled by a factor of $\mathbf{U}_{deeper}/\mathbf{U}_1$,

which was chosen as 0.2 on the experimental basis so that the scaled residuals have approximately the same magnitude on all levels.

The model experiments showed the necessity to use the above scalings. When the model was run with 8 levels without scaling, the diffusive parameters are not resolved (from the noise level) and the equation residuals in the thermocline are much larger than those below. With the scaling, all the parameters are well determined, and all the equation residuals are in the same magnitude. In addition, the solutions on the lowest seven levels are almost identical to the 7-level run without the thermocline level.

When the same weight was given to O_2 as to the θ and S equations, the solutions for the oxygen consumption rate are unreasonably large. This may be due to larger noise in the oxygen data. Comparisons of the Levitus data with the South Atlantic Ventilation Experiment (SAVE) data show large (as large as 0.3 ml/l) offsets in O_2, although the temperature and salinity are consistent. To lessen the possible contamination on the solutions, a small weight (.01) is given to the O_2 equations. Then the consumption rates do not differ significantly from zero.

h. Choice of the rank. Not all the equations are necessarily independent. Since the solutions are proportional to $1/\lambda_i$ (where λ_i are the singular values in the Singular Value Decomposition (SVD, see Strang, 1986) of the matrix G:$G = U\Lambda V^T$), whereas the solution error variances are proportional to $1/\lambda_i^2$, the solution errors blow up much more quickly as the singular values decrease. To get significant solutions, it may be necessary to cut off some small eigenvalues and associated eigenvectors. Wiggins (1972) and Lawson and Hanson (1974) discussed several approaches to determine the effective rank. One method is to display the distributions of the singular values (Fig. 6a), and the real singularity is usually represented by an abrupt drop. Another method is the so-called Levenberg-Marquardt stabilization technique (Fig. 6b), which is used to judge whether small singular values contribute significantly to a reduction in residual variance without inordinate increases in parameter variance. For the current problem, it seems that it is actually full rank and overdetermined. Note that the singular values associated with the conservation equations (the segments with larger slopes at the beginning and the end) are separated by the singular values associated with the nonhomogeneous dynamic equation (3.1) (the segment in the middle with small slope), the dramatic drop at the end of the curve does not imply singularity in this case.

One way to show the individual contribution of the equations to the solutions is to display the data resolution. If $\hat{X}$ is the SVD solution of the true X and $\hat{Y} = G\hat{X}$, one can find (see, e.g., Wunsch, 1978) that $\hat{Y} = UU^TY$, where Y is the true value of $\hat{Y}$. If a diagonal element of UU^T is unity or nearly so, the corresponding equation contributes fully and independently to the solutions. Thus UU^T is called data resolution. For the present problem, Figure 6c shows that the Dynamic Equations are best resolved.

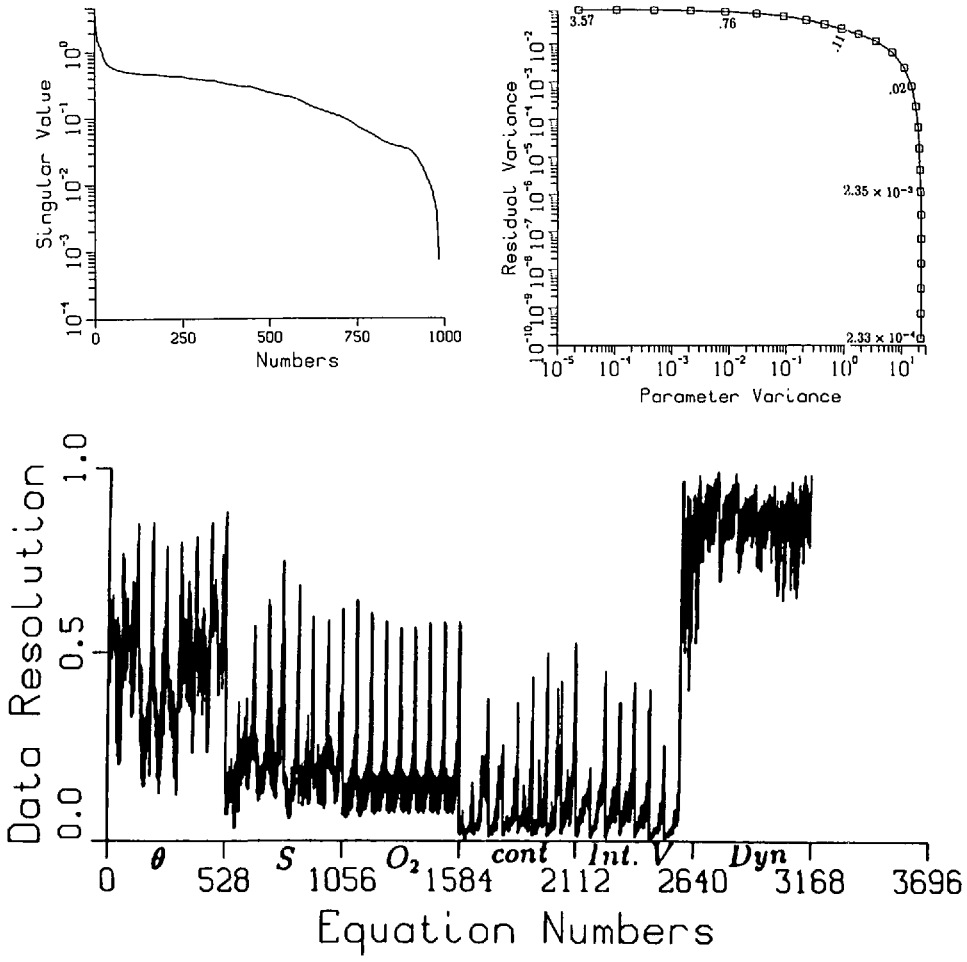

Figure 6. (a) Singular value distributions for the Advective-Diffusive model. (b) Residual variances vs. parameter variances for the Advective-Diffusive model. The values in the diagram are the Levenberg-Marquardt parameters (Lawson and Hanson, 1974), which range from 3.57, the largest singular value in (a), to 2.33×10^{-4}, about one third of the smallest singular value. (c) Data resolutions for the Advective-Diffusive model.

i. Error bounds on the solutions. With the assumption that data noise is not correlated, the error variance for the parameters are determined by (e.g. Wunsch, 1978)

$$E = \epsilon^2 V \Lambda^{-2} V^T \tag{3.10}$$

where ϵ^2 is the expected error determined from the equation residuals.

4. Results and discussions

Three models are proposed for the water property balances in the Brazil Basin, namely the Purely Advective model (PADV), the Advective-Diffusive model with

the same diffusivities for heat and salt (AVDF), and the Double-Diffusive model (i.e. with different diapycnal diffusivities for heat and salt) (DDF). For the PADV model, the results show that there are large-scale significant structures in the equation residuals. This indicates that the water properties cannot be balanced by advection only-some significant physical processes have been left out of the model. Consistent with this, the residuals in the AVDF results are much smaller, and more or less *randomly* distributed (Fig. 13). These small residuals represent the data noise and less important terms left out of the equations. The circulations resulting from the DDF and the AVDF models have not only similar flow patterns, but also similar magnitudes. However, there are some differences in the diffusion parameters. We will depict our results based on the AVDF model first, and then the effectiveness of double diffusion will be explored.

a. Circulations of the water masses in the Brazil Basin

Description of the circulations. The contours of the streamfunction (for $f\mathbf{u}$) on the eight isopycnals are shown in Figure 8. The circulation in the thermocline (level 1, representing the South Atlantic Central Water) has a gyre-like pattern (Fig. 8a), corresponding to the gyre-like pressure contours (Fig. 4a), but the circulation gyre center (at about 10S, 21W) is a little more south than the pressure one. South of 12S, the flows are nearly zonally toward the west, with a speed of about 1.5 cm/s. Nearer the equator (around 5S), flows are zonally toward the east with the velocity of about 3 cm/s. It seems that the gyre system extends to the three immediately lower isopycnals (levels 2, 3, and 4), but the gyre center shifts southward as it deepens. It disappears on the next level (level 5), but water mass analysis (to follow) shows that the southern eastward flow may be the extension of this gyre, centered south of this area.

On the second level, there are also some similarities between the circulation patterns and pressure contours (Fig. 4b). Flowing on this isopycnal is mainly the AAIW: it enters from the southeast corner, and flows almost zonally with velocity at about 1 cm/s in the very south, and farther north it flows northwestward as far as the equatorial region, where it deflects to the northeast, flowing with a velocity of about 1.2 cm/s. Going deeper, since the slopes of the isopycnals become much smaller, the correspondence of the circulation and pressure patterns are no longer apparent. The Upper Circumpolar Water (UCPW, on level 3) also enters from the southeastern region, but with a smaller velocity (about 0.5 cm/s). Some of this water recirculates around a closed cyclonic gyre centered at (22S, 25W), and some of it escapes from the gyre and goes northwestward toward the equatorial region where it meets the oncoming NADW and flows eastward with a velocity of about 1.2 cm/s. The circulation pattern on the next isopycnal (level 4, Fig. 8d) is basically the same as that of the UCPW, except with the center shifted about 3 degrees south.

On level 5, it seems that there are two different flow regimes separated by a very weak flow zone (Fig. 8e). In the north region, water enters from the northwest

$$\nabla_h \cdot (\vec{U}C) - \nabla_h \cdot A\,\nabla_\sigma C - \sigma_z(K\sigma_z C_\sigma)_\sigma + \lambda C + \sigma_z(W^* C)_\sigma = \epsilon$$

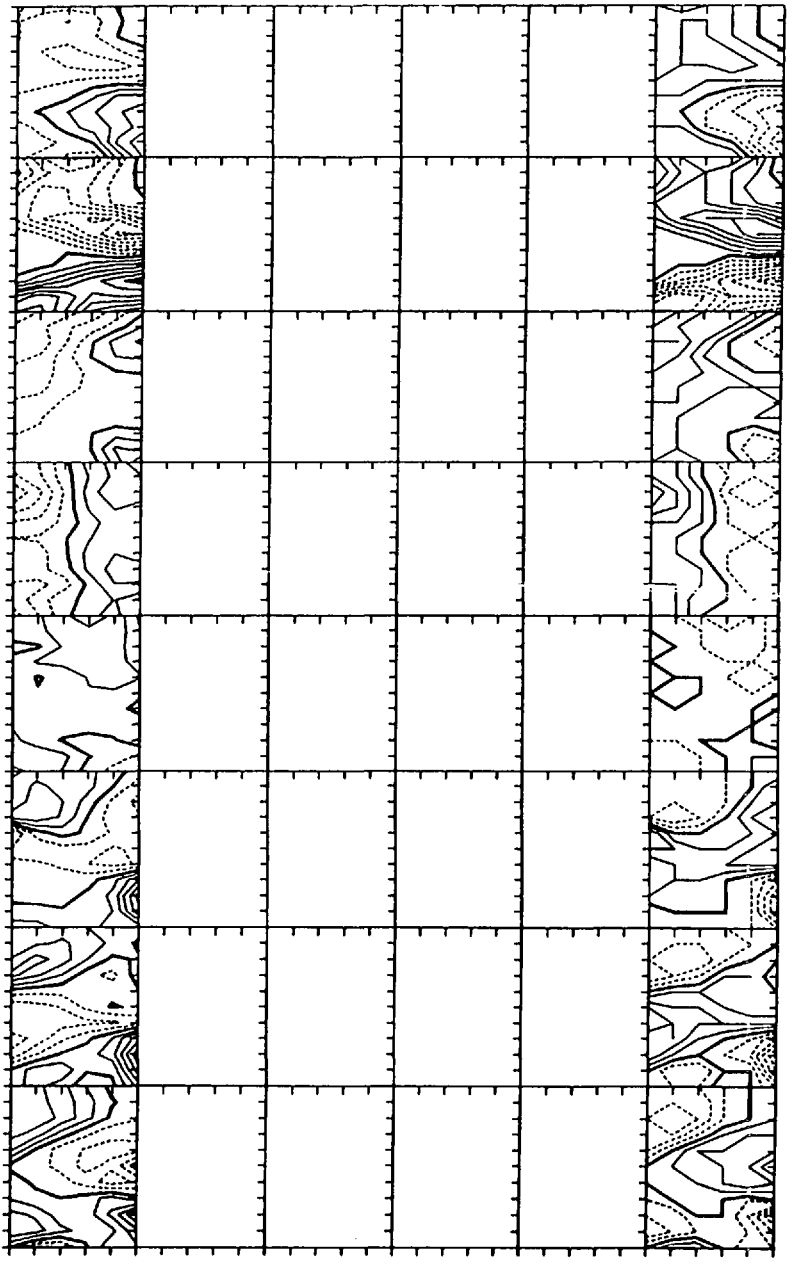

Figure 7. Potential temperature balances on the isopycnals for the Purely-Advective model. C.I. = .01 units. Dashed lines are negative and heavy solid lines are zero.

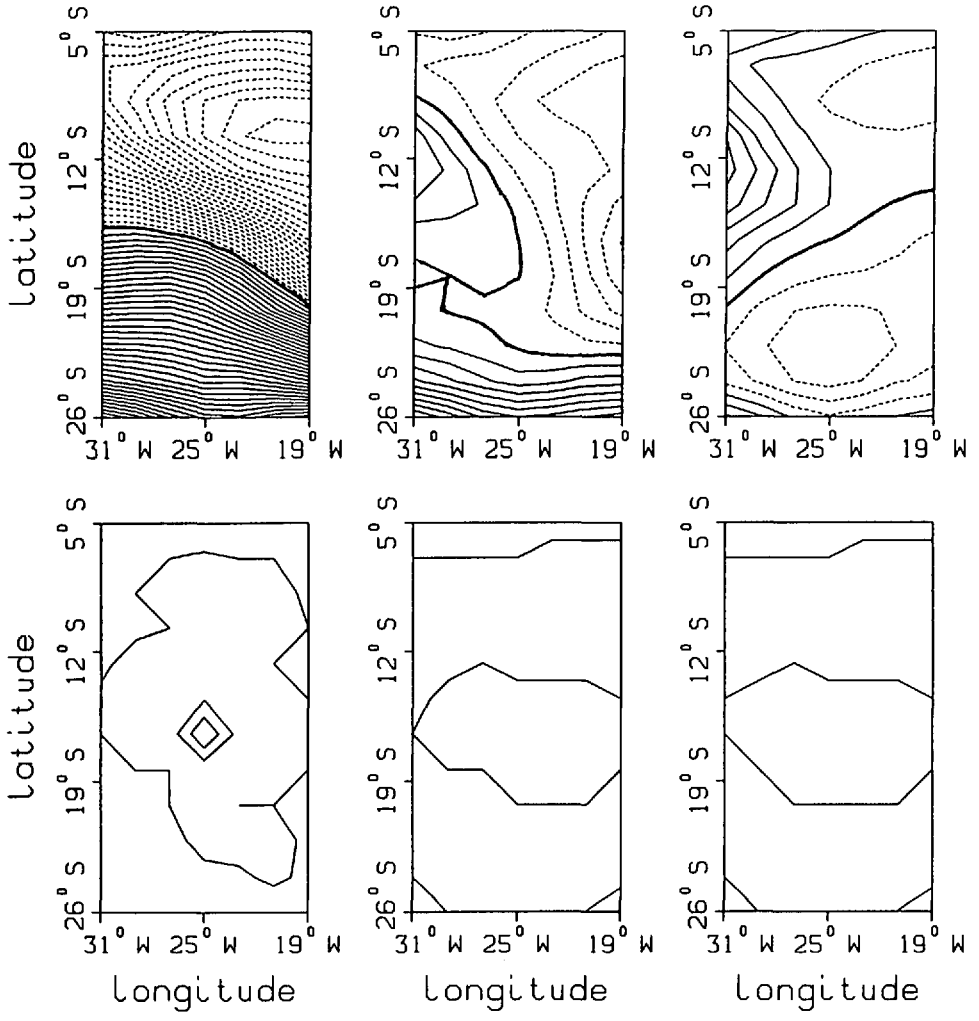

Figure 8. Streamfunctions (upper panel) and their expected errors (lower panel) contours on the 8 isopycnals for the Advective-Diffusive model. (a) level 1; (b) level 2; (c) level 3; (d) level 4; (e) level 5; (f) level 6; (g) level 7; (h) level 8. Dashed lines are negative and heavy solid lines are zero. C.I. = .025 m^2/s^2 for streamfunctions and C.I. = 0.005 m^2/s^2 for their errors with center-most contour of 0.005 m^2/s^2.

corner, flows southeastward with velocity of about 1 cm/s, to 10S and 21W where it turns northeastward. South of 16S flows are almost zonal, and we cannot judge whether they are the extension of the NADW west of the area (31W), as the flows on the lower isopycnals indicate, or they are the recirculating part of the UCPW flow south of the area (26S), as the flows on the upper isopycnal indicates. They can, however, be identified by the water property distributions. In Figure 3, it is noted that there are two different water masses on isopycnal σ_2 = 36.94 (level 5): the warm,

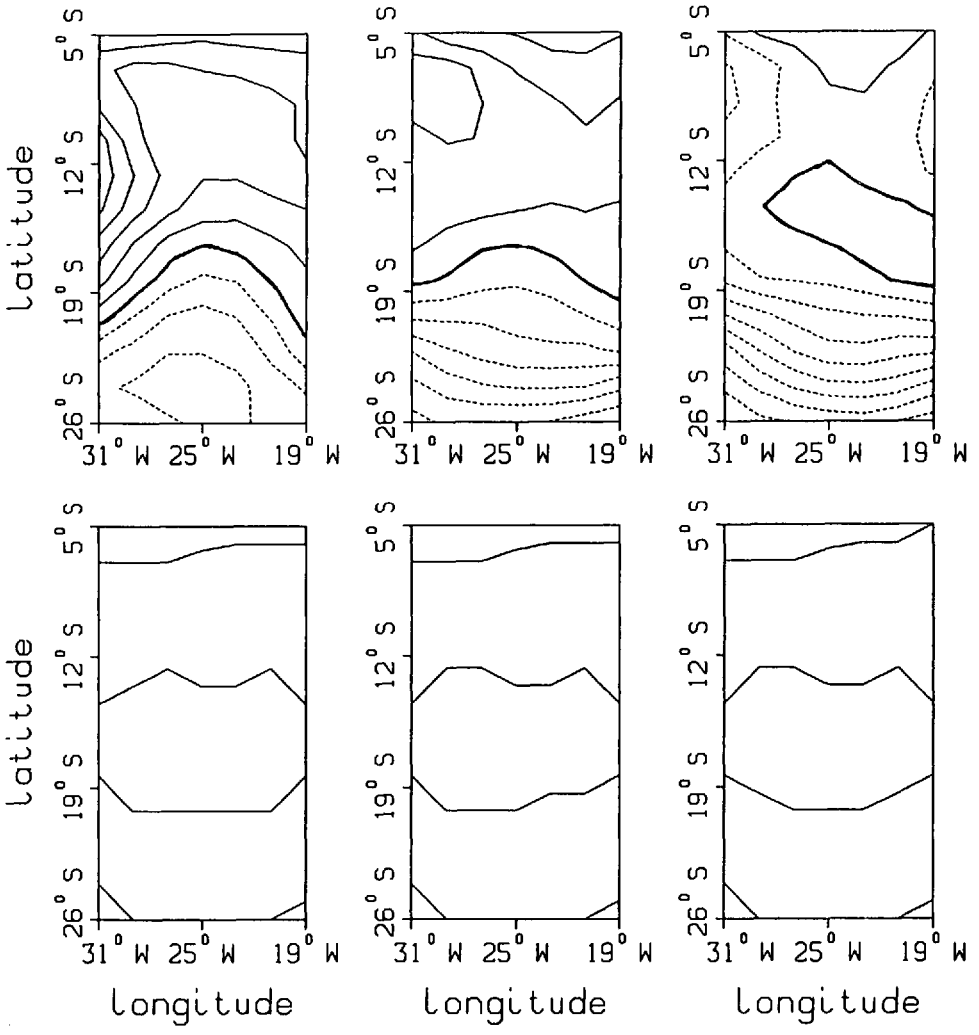

Figure 8. (Continued)

saline and oxygen rich NADW in the north and the cold, fresher and oxygen poor UCPW in the south.

On level 6 lies the center of the salinity maximum, and the potential temperature contours show that the warm NADW extends just to the south edge of this area. This NADW layer is thick and extends downward through the next two levels (level 7 and 8). The circulation patterns of the NADW on these three isopycnals are very similar. The NADW enters this area from the northwest corner, one part of it goes southeastward and then turns northeastward in the north, another part in the west first flows southward and then it deflects eastward in the south, then northeastward. The remaining part of the water recirculates anticyclonically with axis at about 16S, through the region east of this modeled area. As the water recirculates, some of it

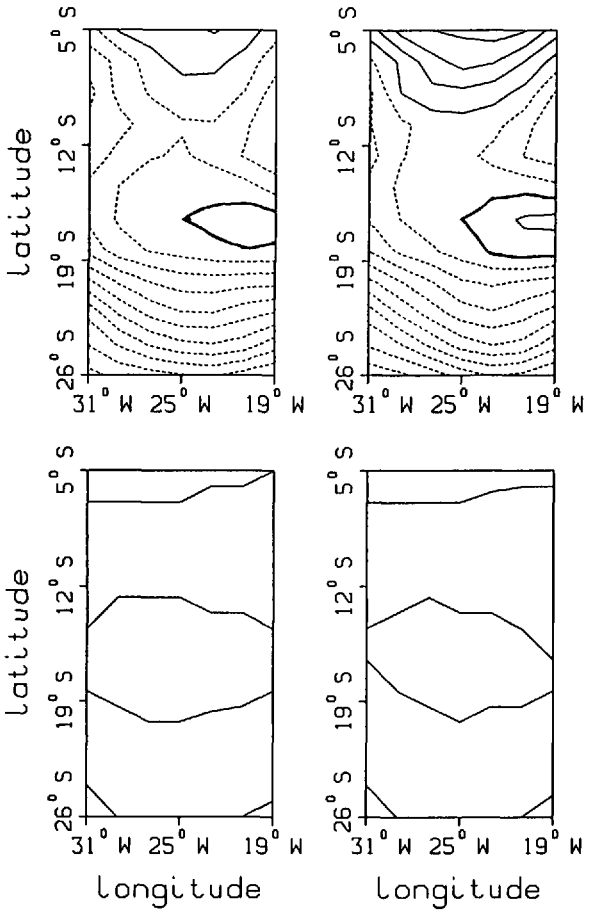

Figure 8. (Continued)

leaves the gyre and bears northward and then joins the northern northeastward flowing NADW.

Comparisons with other work. The very early works on the ocean circulations in the south Atlantic are Wüst's (1935) core layer analysis (Fig. 9) and Defant's (1941) calculations of the absolute flow fields (Fig. 10). Their results are consistent with our NADW flow patterns. Wüst's two tongues correspond to the two strong NADW flows. Defant's absolute flow field is surprisingly similar to ours: the entering NADW from the northwest corner branches in the north, one branch returns to the equatorial region in the north, and the other flows southward first, and deflects to east in the south.

Reid (1989) proposed another method to study the *total* geostrophic flows in the whole South Atlantic Ocean. In the upper ocean, the flows resulting from Reid's calculation and our model are quite consistent. For example, for the near surface

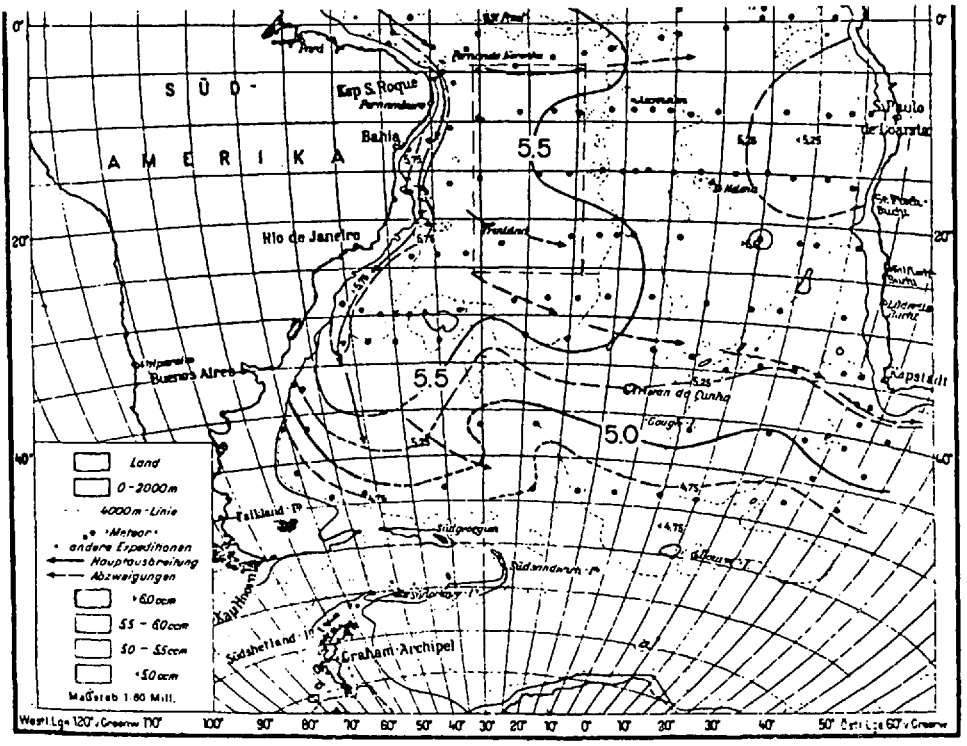

Figure 9. Oxygen (ml/l) of the core layer of the middle North Atlantic Deep Water. (Wüst, 1935).

water, comparison of Reid's adjusted steric height (physically, it's the same as our streamfunction) at 500 dbar (Fig. 11a) with our streamfunction patterns on level 1 (around 500 dbar) shows that both methods give a cyclonic gyre system in this area. Although the detailed structures and velocity values are not exactly the same, the overall velocities are of the same magnitude.

In the deep ocean, the circulation patterns determined from the two different methods are different in detail, but broadly similar in the basin. For example, for the NADW flows, Reid's adjusted steric height at 3000 dbar (Fig. 11b) shows that the NADW has recirculated back to the Brazil Basin from the south, as far south as 50S. In addition, it can also be seen that the flows in this basin are more meridional than zonal, except in the region near the equator. Contrarily, the current model results suggest that the southward flowing NADW along the west boundary (Brazil Coast) is *gradually* deflected to the east and flows into the basin. The most easterly (farthest from the coast) part of the southward flowing NADW (with weaker speed) is deflected first at a relatively northern latitude, and the most westerly part (with stronger speed) is deflected at a relatively southern latitude. Thus the flows in this basin are more zonal than meridional. Some of the differences could well result from Reid's use of selected hydrographic sections as opposed to our use of the highly

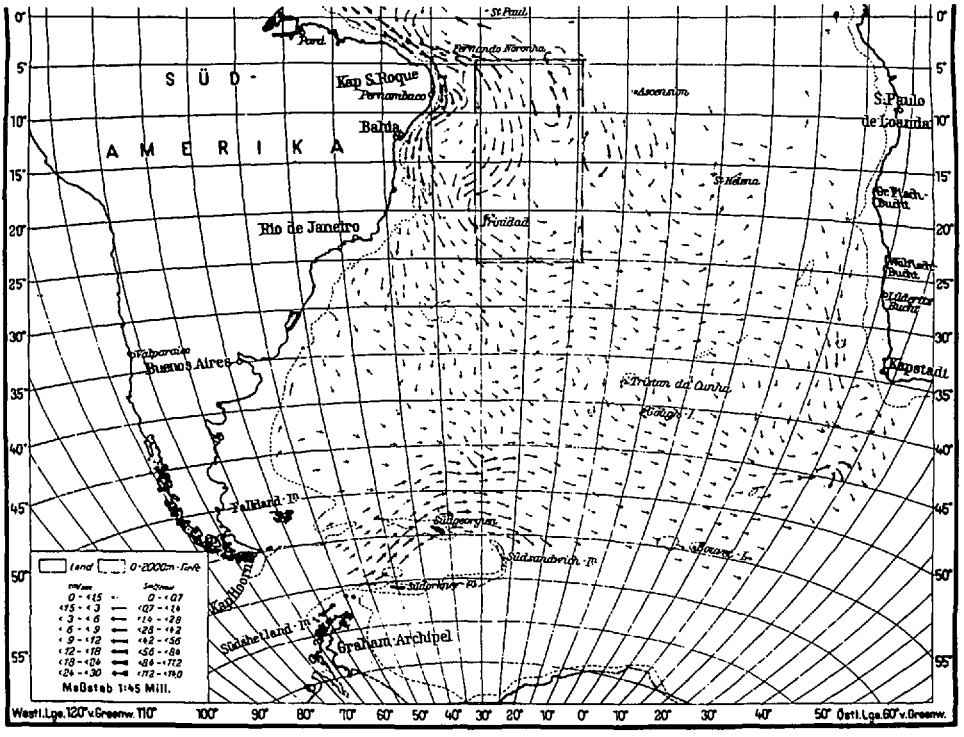

Figure 10. Flow field at 2000 m. (Defant, 1941).

smoothed climatological data. Nonetheless, despite the detail differences, there is a common feature among both model results: the NADW goes firstly southward, deflects to east in the south, then returns to the north, and finally leaves the basin from the northeast corner flowing northeastward after having made the deep southern excursion. It is supposed that this water traverses the mid Atlantic ridge through the equatorial fracture zone passages and enters into the Angola Basin as the source water. The current model results also suggest that the entering NADW most likely has come through the Ceara Abyssal Plain passage.

Fu (1981) used the geostrophic box inverse model to study the general circulation and meridional heat transport of the subtropical South Atlantic Ocean. This method is good for determining the velocities and property transports *across* the vertical sections, but not for studying the detailed horizontal circulation structures. However, it is of interest to examine any similarities or differences in the major features. For the IGY data set, Fu's circulations for the Surface Water, the AAIW, and the UCPW do have some similarities to our and Reid's results, whereas the circulations for the deep water are different from both. For the *Meteor* data set, Fu's circulation pattern for the lower NADW has some similarity to ours, both different from Reid's almost meridional flow.

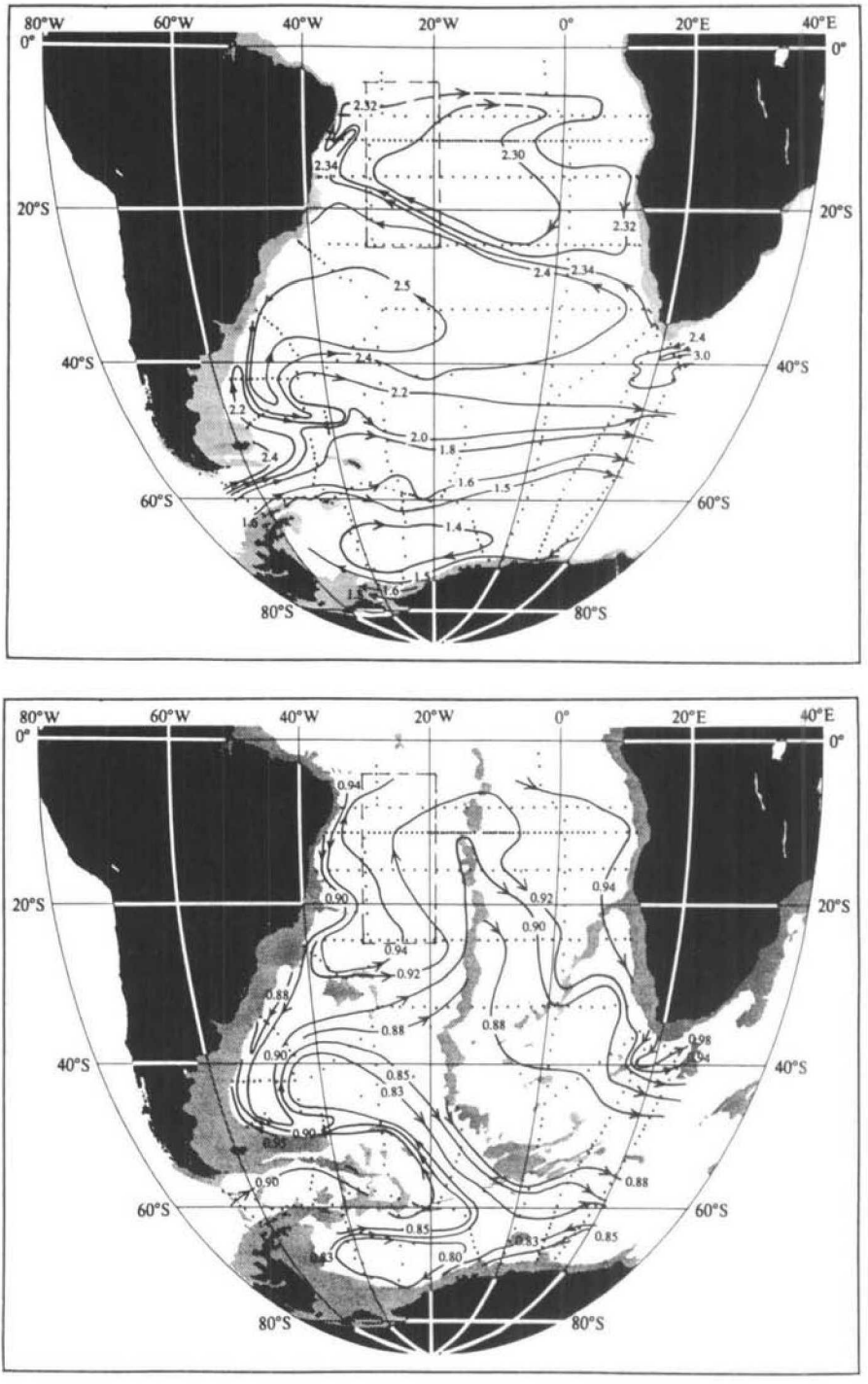

Figure 11. Adjusted steric height (10 m^2/s^2) at (a) 500 db; and (b) 3000 db. (Reid, 1989).

b. Diffusive parameters

The isopycnal and diapycnal diffusivities (A,K), diapycnal velocities (w^*) and oxygen consumption rates (λ) are shown in Figure 12. The isopycnal diffusivities have maximum values of $10^4 m^2/s$ on level 4, and the aerial average is of order $10^3 m^2/s$. The eddy diffusivities are obviously not uniform in the area, and a general trend is that they are larger in the north (near equator) than in the south. This implies that the eddy activities in the near equatorial region are stronger, consistent with Wyrtki *et al.* (1976)'s eddy energy distribution map. The diapycnal diffusivities have a maximum value of about $20 \times 10^{-4} m^2/s$, which appears at the northwest corner on the bottom level (the lower NADW). The aerial averaged values are of $10 \times 10^{-4} m^2/s$, of the same order of magnitude computed by Hogg *et al.* (1982) using heat and mass balances for the bottom water of the Brazil Basin. The diapycnal velocities have the magnitude of 10×10^{-7} m/s, and the extreme value can be as large as 70×10^{-7} m/s, which also appears on the deepest level. The lateral structures are similar to those of the diapycnal and isopycnal diffusivities in the main features. There is "downwelling" on the top three levels, "upwelling" on the next four levels, and "downwelling" again on the bottom level.

There is a vast body of literature on different estimation methods for the eddy diffusivities in the ocean, with a wide range of values (Munk, 1966; Fiadeiro and Craig, 1978; Gregg, 1987; Gargett, 1986, 1989; Spitzer and Jenkins, 1989; Olbers *et al.*, 1985). Generally, the so called eddy diffusivities are model and data set dependent, therefore one cannot expect to find *universal* or *constant* values for them. Our values are in the range of previous works.

c. Water mass balances

Currents generally do not flow along the isopleths of water properties. As shown before, the Purely Advective model is not sufficient for the property balances in the basin; mixing processes are also important in the modifications of water properties.

On level 1, there is a dipole structure in the temperature (salinity) contour (Fig. 4c): a hot (saltier) center near (22W, 8S) in the north and a cooler (fresher) center near (25W, 18S) in the south. The flows are generally down the temperature (salinity) gradient in the southeast, and against the gradient in the other regions. Therefore in the southeast, currents advect hot water and thus have the tendency to heat up the downstream, cooler region. The steady field must be maintained by cooling processes, which are mainly accomplished by the upwelling of cooler deep waters, as shown in Figure 12a (top panel). In the regions other than the southeast, the water is generally warmed up on its way, and the warming is mainly balanced by downwelling in those regions.

The interpretation of the *isopycnal* processes for salinity is the same as for temperature. However, despite the along isopycnal similarities between temperature and salinity contours, the diapycnal gradients may be very different, thus the importance of the diapycnal processes may be different. For example, the salt balance maps (Fig. 13b) show that diapycnal advection is ineffective on levels 2, 5,

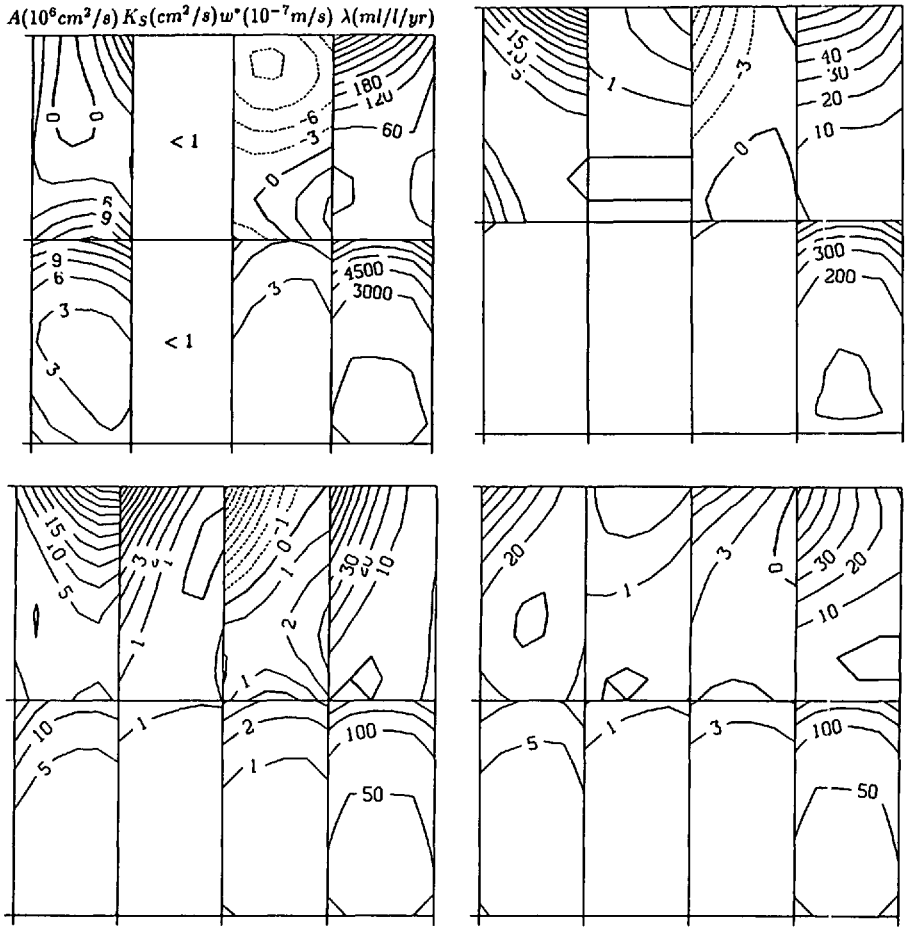

Figure 12. Solutions (upper panel) and their expected errors (lower panel) of diffusivities (A, K), diapycnal velocities (w^*) and oxygen consumption rates (λ) for the Advective-Diffusive model. (a) level 1; (b) level 2; (c) level 3; (d) level 4; (e) level 5; (f) level 6; (g) level 7; (h) level 8.

and 7, but important in the temperature balances (Fig. 13a). On the other hand, on levels 3 and 4, the diapycnal advection are effective in the salt balances but not in the temperature balances.

On level 2 for the AAIW, all four processes, namely the lateral and diapycnal advections and diffusions, are in effect in the temperature balance (Fig. 13a, 2nd panel). On levels 3 and 4 for the UCPW, the temperature (and salinity) contours are very similar to each other (Fig. 4e and Fig. 4f). However they arise from different processes, as shown in Figure 13a (and Fig. 13b): on level 3, the balance is mainly between the *advection* processes (lateral and diapycnal advections), while on level 4, the balance is mainly between *isopycnal* processes (lateral advection and diffusion).

Basically, on levels 6, 7 and 8 for the NADW, all the processes are important in the

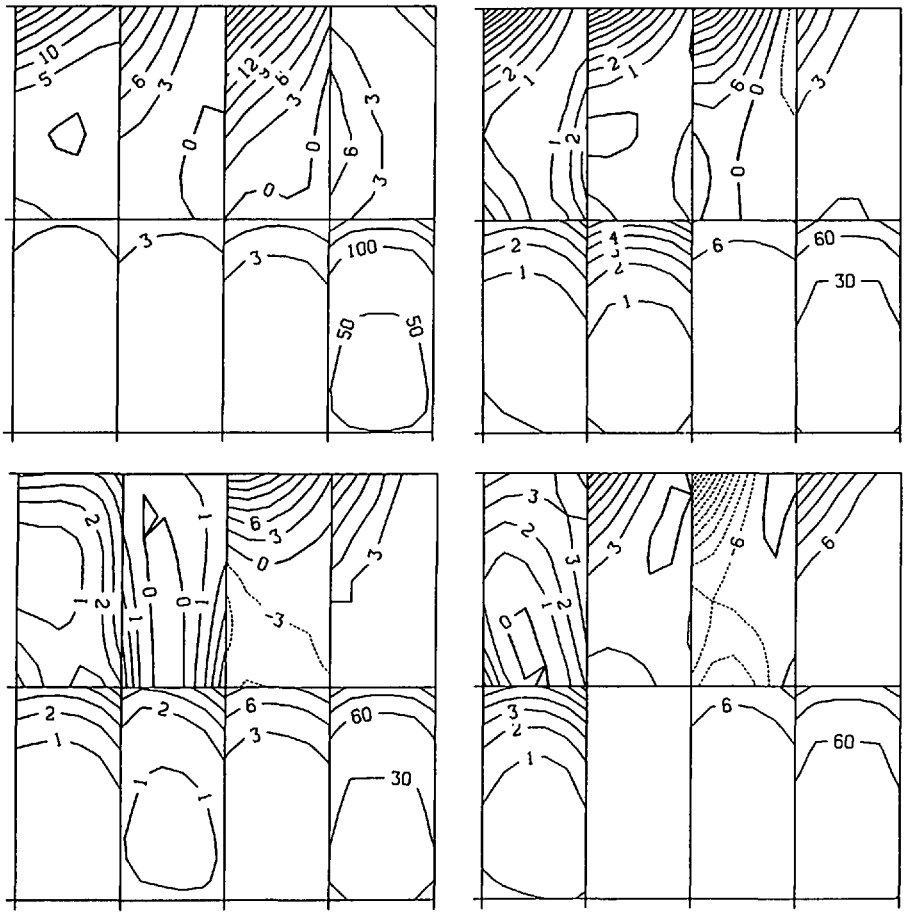

Figure 12. (Continued)

property balances, some more important in one region than another. As well as the similarities of the circulation patterns, the temperature (salinity, oxygen) contours are also very similar on all the three isopycnals. A close correlation between the circulation patterns and property contours can be identified. The anticyclonic gyre corresponds to the cold, fresher center (Fig. 4g), with the gyre center just south of the cold center. If one draws a line along the cold, fresh tongue, one can find that this line is just in the position of the northwestward flowing current and just north of the gyre center. In the south, the direction of the warm, saltier tongue corresponds to the strong southeastward flow. Thus without *a priori* prejudice toward forcing the flows to go along the tongues of the water properties, we do find the coincidence. The core-layer method cannot tell us the details of the flows especially when tongues become weaker and disappear. But our flow fields can tell us about this. For example, the cold, fresh water first goes along the tongue, and when the tongue weakens, the water leaves the tongue. In the north it flows toward the northeast and finally joins

$$\nabla_h \cdot (\vec{U}C) - \nabla_h \cdot A \nabla_\sigma C - \sigma_z(K\sigma_z C_\sigma)_\sigma + \lambda C + \sigma_z(W^* C)_\sigma = \epsilon$$

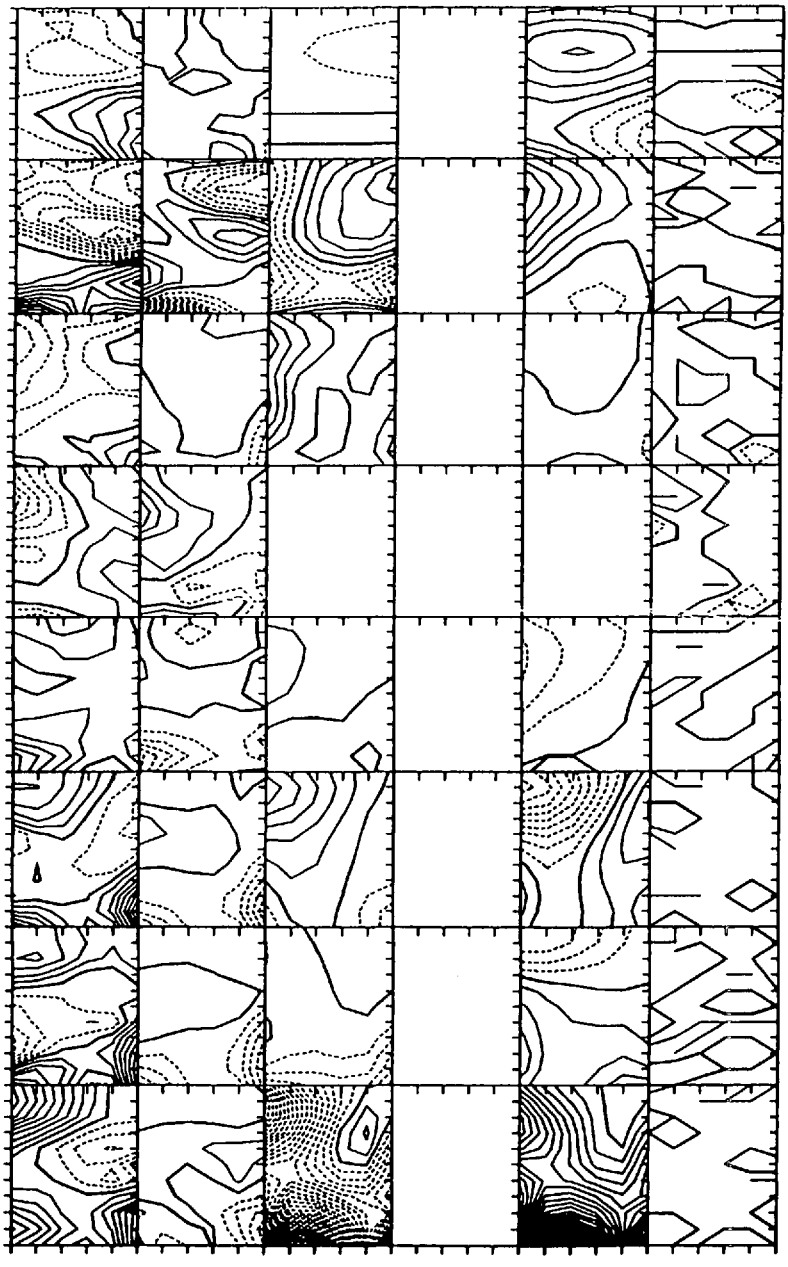

Figure 13. (a) Potential temperature balances on the isopycnals for the Advective-Diffusive model. The eight rows in the vertical represent the eight isopycnals, and the six columns represent the five terms in the conservation equation and their residual as shown at the top. C.I. = .01 units. Dashed lines are negative and heavy solid lines are zero. (b) Same as (a) but for salinity balances. C.I. = .005. (c) Same as (a) but for oxygen balances. C.I. = .005. (d) Continuity balances on the isopycnals for the Advective-Diffusive model. C.I. = .005. (e) Integrated vorticity balances between the isopycnals for the Advective-Diffusive model. C.I. = .005. (f) Dynamic equation balances between the isopycnals for the Advective-Diffusive model. C.I. = .5.

$$\nabla_h \cdot (\vec{U}C) - \nabla_h \cdot A \nabla_\sigma C - \sigma_z (K \sigma_z C_\sigma)_\sigma + \lambda C + \sigma_z (W^* C)_\sigma = \epsilon$$

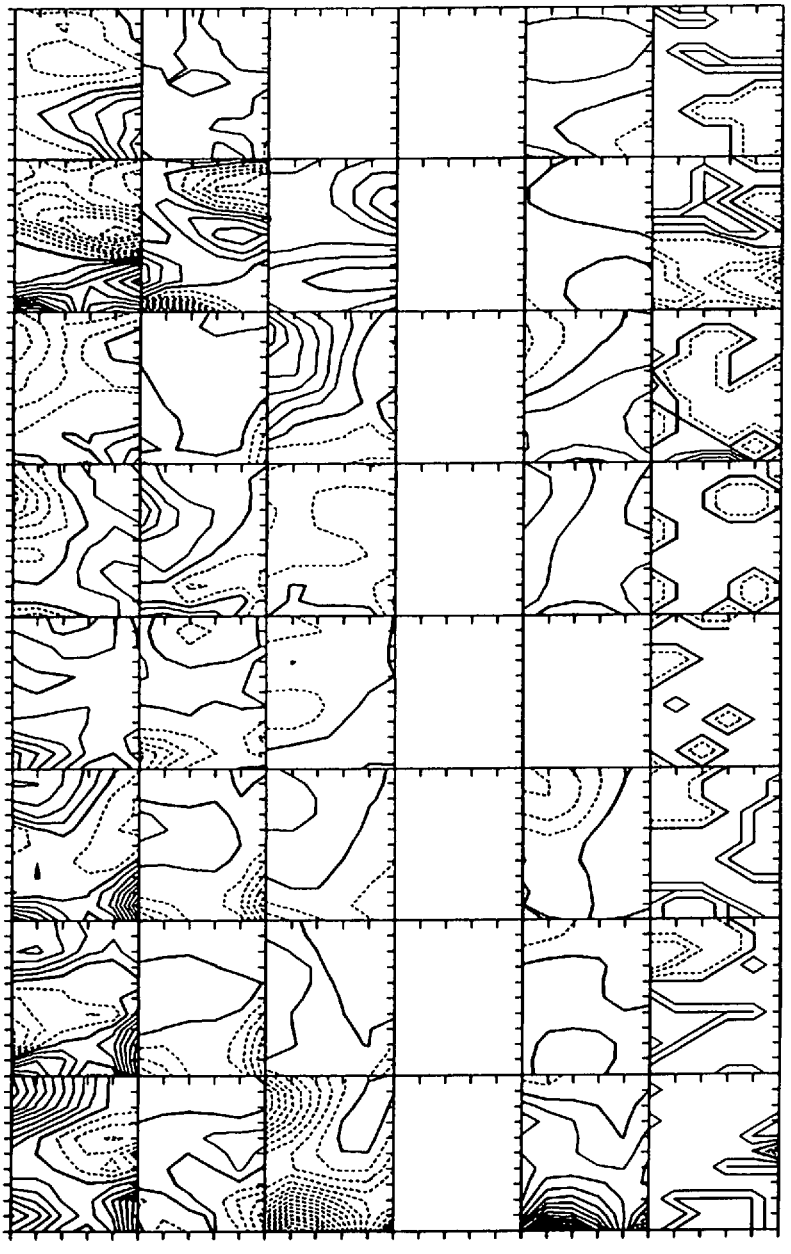

Figure 13 (b). (Continued)

$$\nabla_h \cdot (\vec{U}C) - \nabla_h \cdot A \nabla_\sigma C - \sigma_z (K \sigma_z C_\sigma)_\sigma + \lambda C + \sigma_z (W^* C)_\sigma = \epsilon$$

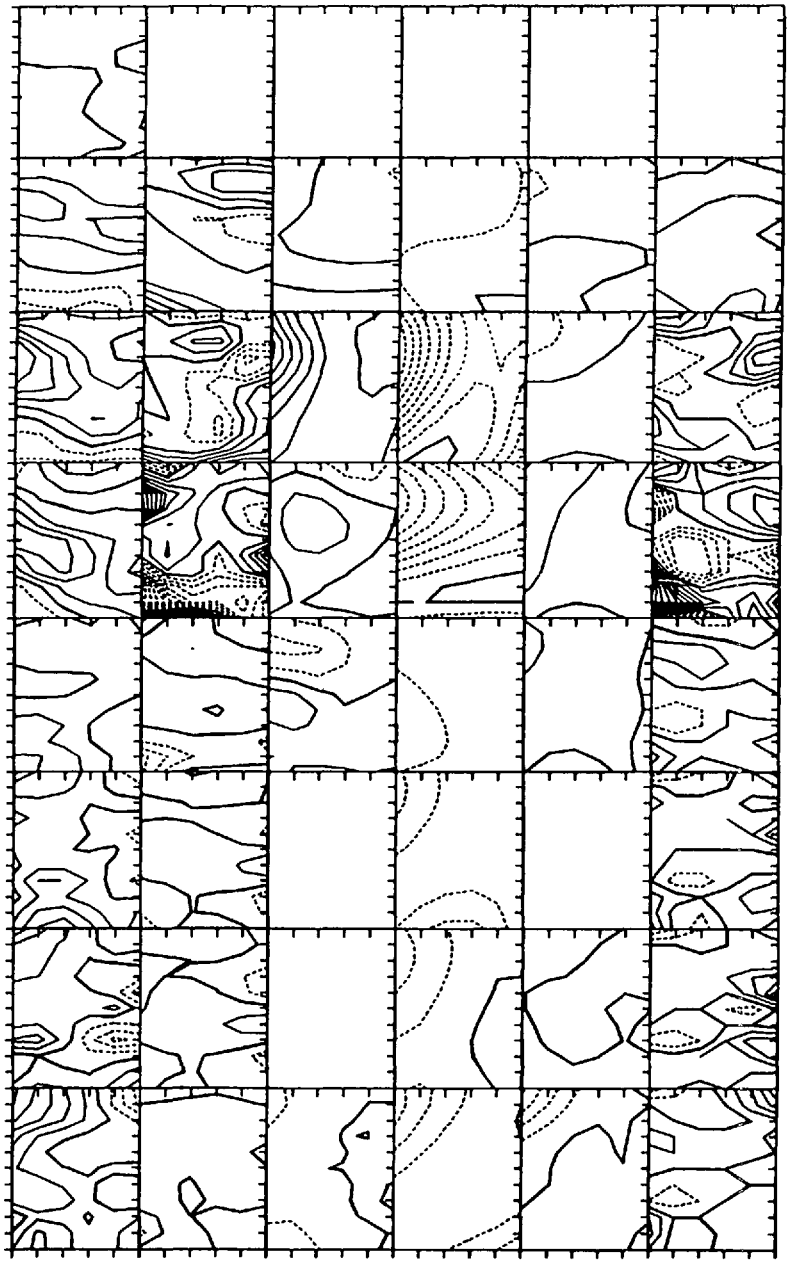

Figure 13 (c). (Continued)

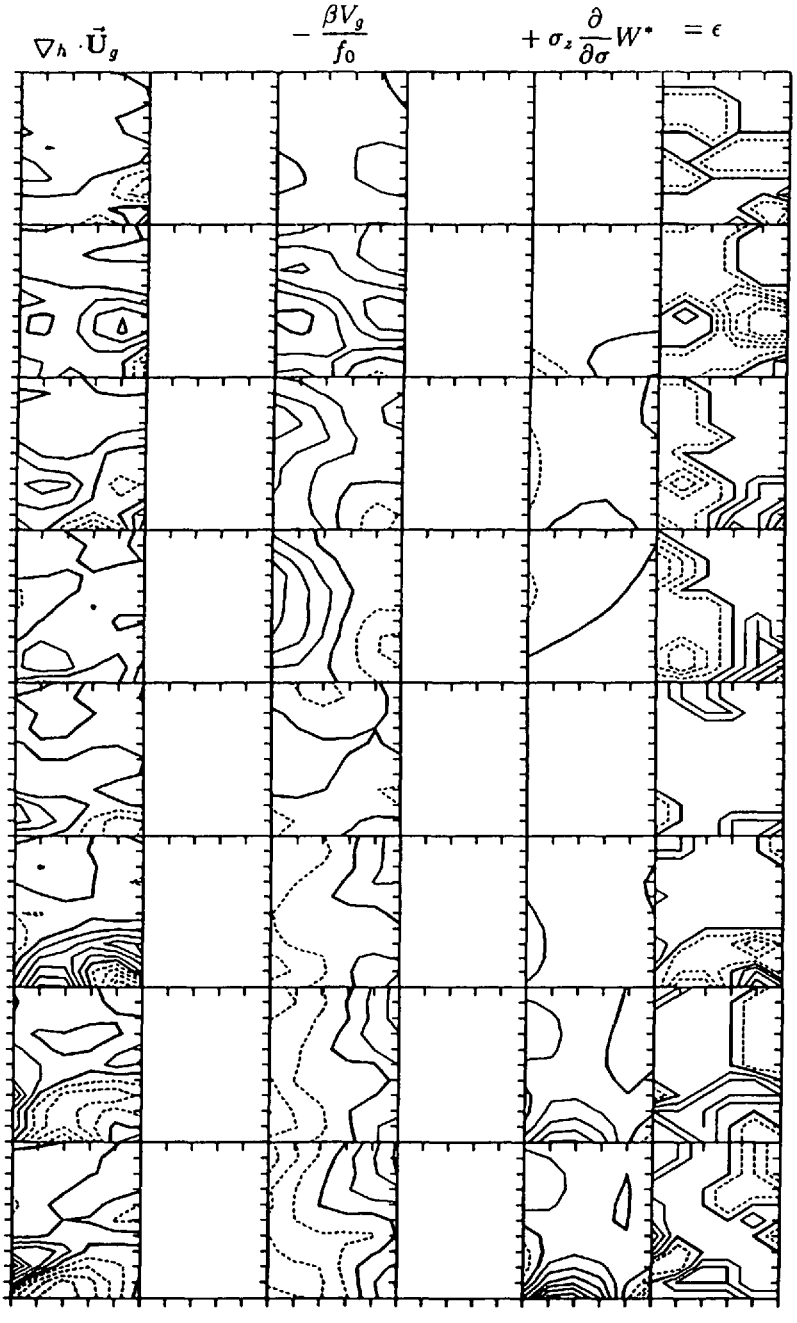

Figure 13 (d). (Continued)

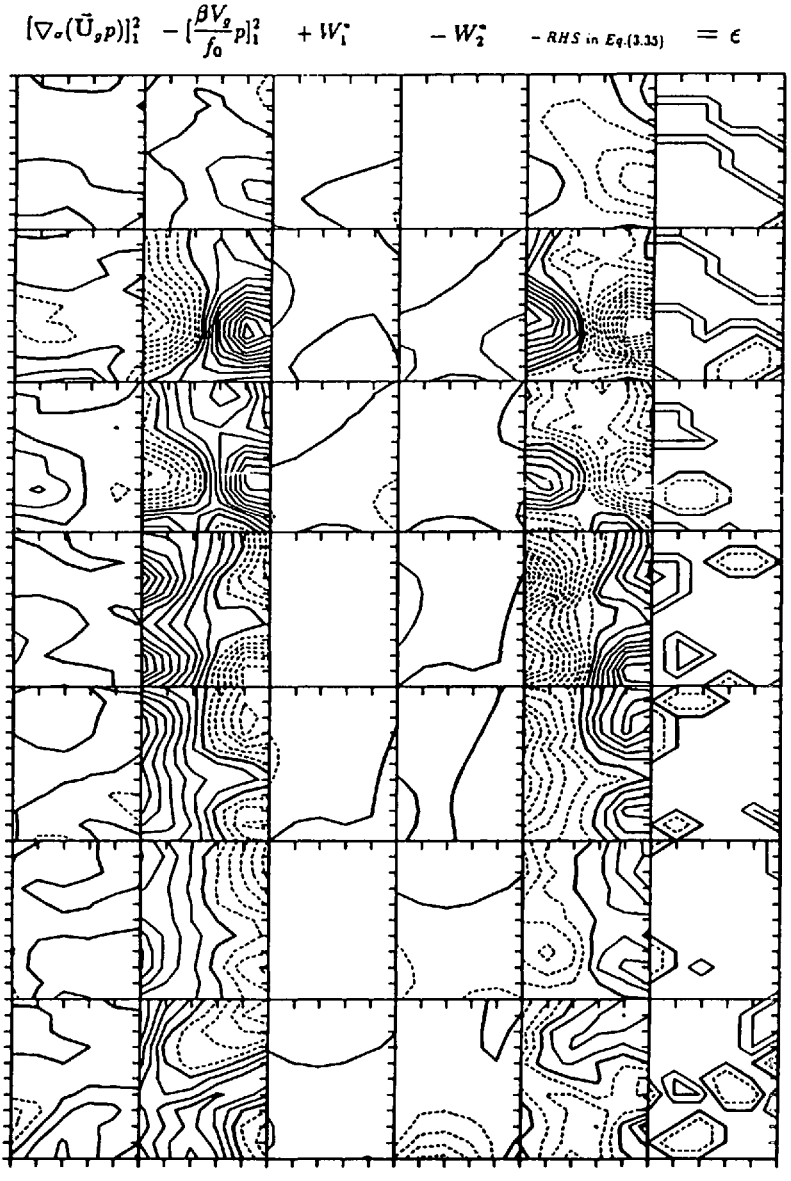

Figure 13 (e). (Continued)

the northern northeast flowing NADW (there the flows are almost along the isotherms). In the south, the leaving tongue water flows southeastward and joins the southeast flowing current of NADW (In the very south, the flow direction is also nearly along the isotherms).

Balances in the continuity equation. In the formulation of the continuity equation, we have expanded the 3-D nondivergence into three terms: isopycnal divergence term,

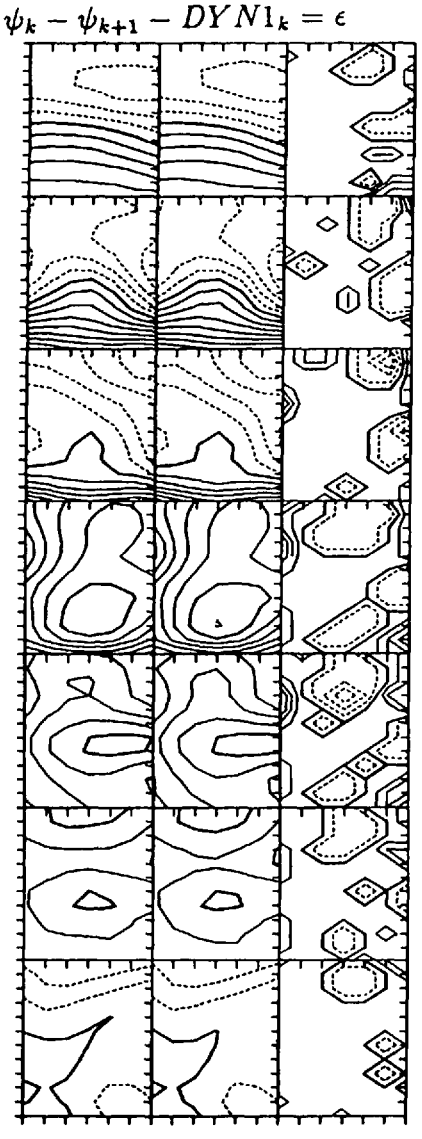

Figure 13 (f). (Continued)

planetary divergence term, and diapycnal divergence term. The balance of these terms are shown in Figure 13d, and it can be seen that on most of the isopycnals (all except level 8), the balances are mainly between the lateral processes: lateral divergence balances the planetary divergence.

Integrated vorticity balances. There are the following terms in the integrated vorticity equation (Eq. (3.3)): the diapycnal velocity difference (diapycnal stretching), the difference of isopycnal advection of p (or z), or the *vertical* velocity

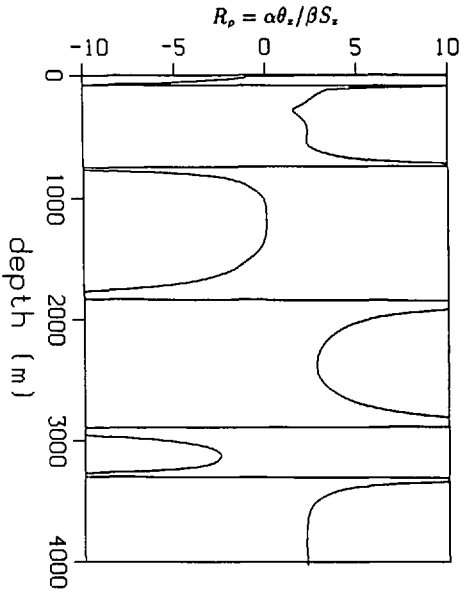

Figure 14. Profile of the stability parameter R_ρ at (26.5W, 6.5S).

difference resulting from the flows along sloping isopycnals (vertical stretching), the difference of the advection of the planetary vorticity, and the right hand side (RHS) inhomogeneous term associated with the sloping effects of specific volume anomaly and pressure along isopycnals. These terms are shown in Figure 13e, and it can be seen that the balance is mainly between the advection of the planetary vorticity and the RHS inhomogeneous term.

Balances in the dynamic equation. The terms in the Dynamic Equation, Eq. (3.1), are plotted in Figure 13f. The first column is the streamfunction difference between two isopycnals, and the second column is the terms on the RHS—the theoretical difference for the streamfunctions. The similarities of these two terms and the small residuals assure us that the thermal wind relation is well satisfied by the computed flows.

d. Effects of double diffusion

The profiles of the stability parameter R_ρ ($R_\rho = \alpha\theta_z/\beta S_z$), which is the ratio of the relative contributions of heat and salt to the density flux (see Schmitt, 1990), in the Brazil Basin (Fig. 14) indicate that there are several *potential* double diffusion regions. To reveal its real importance (since other processes, such as wave breaking, cabbeling, etc., may also be important) in the water property balances, we ran the 8 level model with different unknowns for K_T and K_S. The results show that as far as the circulations are concerned, there are no significant differences in the single and double diffusive models. For the lateral diffusion coefficient A, the two model results are also not significantly different. From the solutions for K_T and K_S and their expected errors, it can be seen that the real significant differences between K_T and K_S

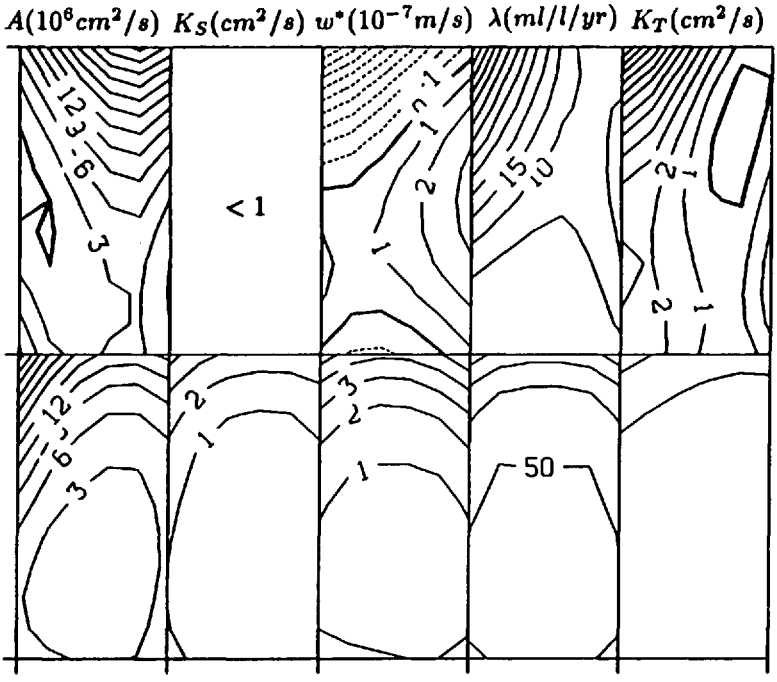

Figure 15. Solutions (upper) and their expected errors (lower) of diffusivities (A, K_T, K_S), diapycnal velocities (w^*) and oxygen consumption rates (λ) for the Advective-Diffusive model on level 3.

are obtained on level 3, on which $K_T > K_S$ (Fig. 15). Corresponding to this level is a thin, weak inversion in temperature and a strongly stable salinity profile, so that the stability parameter R_ρ falls into the diffusive double diffusion regime. $K_T > K_S$ is thus implied.

There is another way to determine the effectiveness of the double diffusive mixing, i.e. by looking at the θ-S relations. If double diffusion is not effective (compared with other mixing processes), the eddy diffusivities for temperature and salinity are the same, and the θ-S relation tends to be linear. On the other hand, in regions of effective double diffusion, the θ-S relation tends to be along constant stability ratio (R_ρ = *const*), or $\alpha\theta$-βS tends to be linear (Ingham, 1966; Schmitt, 1981, 1990). The linearness of the θ-S and $\alpha\theta$-βS profiles shows the competition between the double diffusion and turbulent processes. Some of these profiles at (28.5W, 6.5S) in the several *potential* double diffusion ranges are shown in Figure 16. It can be seen that only in the region where the temperature inversion appears, the $\alpha\theta$-βS relation is more linear.

5. Conclusions

Potential density analysis has long been used in descriptive oceanography, based on the assumption that water properties are advected mainly along isopycnal

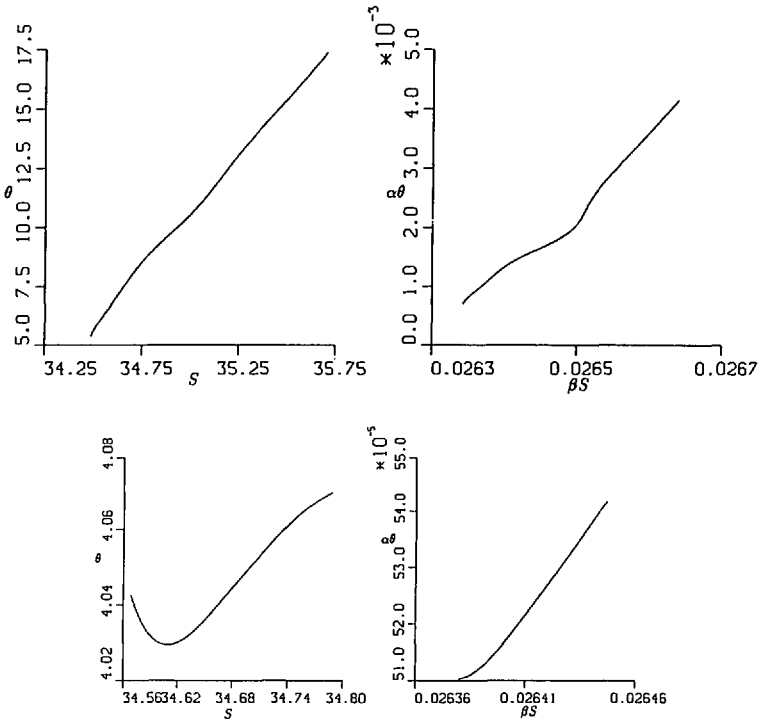

Figure 16. θ-S (left) and αθ-βS (right) relations between (a) 150–650 m; and (b) 1000–1250 m.

surfaces. Potential density coordinates have also been widely used recently in dynamic models. Some streamfunctions for certain vertical coordinates have been derived, but an exact form for potential density coordinates does not exist. The application of the Montgomery streamfunction to the potential density coordinates produces large errors in some regions in the ocean. By including the major part of this error term the so called pressure anomaly and mean pressure streamfunctions are suggested for use in potential density coordinates, in which the leftover part induces errors in velocity no larger than 10%. From their formulations, these streamfunctions can also be used in other gently sloping surfaces without producing large errors.

The inverse model used in this work comprises the dynamic method and water property conservations as in most of the inverse models. But in this model, equations are written in the point-wise basis in potential density coordinates, in which are implied water mass conservation over small volumes (boxes). Thus detailed circulations and mass balance processes can be studied. The current model results for the circulations for the upper levels in the Brazil Basin show consistency with previous works, but those at the deep levels are consistent with some works and different from others. On the upper levels, there is a cyclonic gyre in the Brazil Basin, and the gyre center migrates southward as it deepens. There is a close correlation between the

circulation patterns and pressure contours, however this correlation is not apparent on the deep levels. The flows are generally stronger in the region near the equator than in the south. For the deep water, the present results show that the southward flowing NADW along the western boundary gradually turns to the east into the Brazil Basin from north to south, and in the north the NADW leaves the basin northeastward and may traverse the mid-Atlantic ridge through the equatorial fracture zone passages and enter the Angola Basin as the source water for that basin. Examples of the coincidence of the flow paths with the tongues of water properties are also found.

The magnitudes of the diffusivities and diapycnal velocities differ from place to place: larger in the equatorial region than in the south, which is consistent with the previous study on eddy energy distributions. The values are in the ranges of their magnitudes in the literature. Since the flows are generally not along the isopleths of water properties, the steady fields must be maintained by diffusive processes as well. Similar property fields at different depths and in different areas may result from quite different processes.

Acknowledgments. We would like to thank Carl Wunsch, Harry Bryden, Mike McCartney, Breck Owens, Ray Schmitt and William Jenkins for helpful discussions and comments. Trevor McDougall and a reviewer are thanked for their careful reading of the manuscript and their useful comments and suggestions. Part of this work was realized on the MIT CRAY system. This research was supported by the Office of Naval Research through grant N00014-90-J-1465 and the National Science Foundation through grant OCE-9004396. This is contribution number 7909 from the Woods Hole Oceanographic Institution.

REFERENCES

Armi, L. 1979. Effects of variations in eddy diffusivity on property distributions in the ocean. J. Mar. Res., *37,* 525–530.

Armi, L. and D. B. Haidvogel. 1982. Effects of variable and anisotropic diffusivities in a steady-state diffusive model. J. Phys. Oceanogr., *12,* 785–794.

de Boor, C. 1978. A Practical Guide to Splines, Springer-Verlag, New York, 392 pp.

Defant A. 1941. Quantitative Untersuchungen zur Statik und Dynamik des Atlantis-chen Ozeans. Die absolute Topographie des physikalischen Meeresniveaus und der Drück-flachen sowie die Wasserbewegungen im Raum des Atlantischen Ozeans *in* Wissenschaft-liche Ergebnisse der Deuschen Atlantstchen Expedition auf dem Forschungsund vermess-ungsschiff "Meter" 1925–1927, 6, 2nd Part, 1, 191–260.

Fiadeiro, M. E. and H. Craig. 1978. Three-Dimensional modeling of tracers in the deep Pacific Ocean: I. Salinity and oxygen. J. Mar. Res., *36,* 323–355.

Fu, L. L. 1981. The general circulation and meridional heat transport of the subtropical South Atlantic determined by inverse methods. J. Phys. Oceanogr., *11,* 1171–1193.

Gargett, A. E. 1986. An investigation of the occurrence of oceanic turbulence with respect to finestructure. J. Phys. Oceanogr., *6,* 139–156.

——1989. Ocean turbulence. Ann. Rev. Fluid Mech., *21,* 419–451.

Gregg, M. C. 1987. Diapycnal mixing in the thermocline: a review: J. Geophys. Res., *92,* 5249–5286.

Hogg, N. 1987. A least-squares fit of the advective-diffusive equations to Levitus atlas data. J. Mar. Res., *45,* 347–375.

Hogg, N., P. Biscaye, W. Gardner and W. J. Schmitz, Jr. 1982. On the transport and modification of Antarctic Bottom Water in the Vema Channel. J. Mar. Res., *40,* 231–263.

Ingham, M. C. 1966. The Salinity Extrema of the World Ocean. Ph.D. Dissertation, Oregon State University, Corvallis, OR, 123 pp.

Lawson, C. L. and R. J. Hanson. 1974. Solving Least Squares Problems, Prentice-Hall, Inc., Englewood Cliffs, NJ, 340+xii pp.

Levitus, S. 1982. Climatological Atlas of the World Ocean, NOAA Professional Paper 13, National Oceanic and Atmospheric Administration, Rockville, MD 173+xv pp.

McDougall, T. J. 1987. Neutral surfaces. J. Phys. Oceanogr., *17,* 1950–1964.

——1989. Streamfunction for the lateral velocity vector in a compressible ocean. J. Mar. Res., *47,* 267–284.

Montgomery, R. B. 1938. Circulation in upper layers of southern North Atlantic deduced with use of isentropic analysis. Paps. Phys. Oceanogr. Meterol., *6,* 2, 55 pp.

Munk, H. M. 1966. Abyssal recipes. Deep-Sea Res., *63,* 707–730.

Olbers, D. J., M. Wenzel and J. Willebrand. 1985. The inference of North Atlantic circulation patterns from climatological data. Rev. Geophys., *23,* 313–356.

Pond, S. and G. Pickard. 1983. Introductory Dynamical Oceanography, 2nd edition, Pergamon Press, 329+xx pp.

Reid, J. 1989. On the total geostrophic circulation of the South Atlantic Ocean: Flow patterns, tracers, and transports, Prog. Oceanogr., *23,* 149–244.

——1980. On the Mid-depth circulation of the world oceans, *in* Evolution of Physical Oceanography, B. A. Warren and C. Wunsch, eds., The MIT Press, 623+xxxiv pp.

Schmitt, R. W., Jr. 1981. Form of temperature-salinity relationship in the Central Water: Evidence for double-diffusion mixing. J. Phys. Oceanogr., *11,* 1015–1026.

——1990. On the density ratio balance in the Central Water. J. Phys. Oceanogr., *20,* 900–906.

Spitzer, W. S. and W. J. Jenkins. 1989. Rates of vertical mixing, gas exchange and new production: Estimates from seasonal gas cycles in the upper ocean near Bermuda. J. Mar. Res., *47,* 169–196.

Stommel, H. and F. Schott. 1977. The beta spiral and the determination of the absolute velocity field from hydrographic station data. Deep-Sea Res., *24,* 325–329.

Strang, G. 1986. Introduction to Applied Mathematics, Wellesley-Cambridge Press, Wellesley, MA, 758 pp.

Wiggins, R. A. 1972. The general linear inverse problem: Implication to surface waves and free oscillation on earth. Rev. Geophys., *10,* 251–285.

Wright, R. 1969. Deep water movement in the Western Atlantic as determined by use of a box model. Deep-Sea Res., *16,* 433–446.

Wunsch, C. 1977. Determining the general circulation of the ocean: A preliminary discussion. Science, *196,* 871–875.

——1978. The general circulation of the North Atlantic west of 50W determined from inverse methods. Rev. Geophys. Space Phys., *16,* 583–620.

Wüst, G. 1935. Schichtung und Zirkulation des Atlantischen Ozeans. Die Stratosphäre *in* Wissenschaftliche Ergebnisse der Deuschen Atlantstchen Expedition auf dem Forschungs und vermessungsschiff "Meter" 1925–1927, 6, 1st Part, 2, 180 pp.

Wyrtki, K., L. Magaard and J. Hager. 1976. Eddy energy in the oceans. J. Geophys. Res., *81,* 2641–2646.

Received: *7 January, 1992;* revised: *4 May, 1992.*